

A selection of hot subluminous stars in the *GALEX* survey

I. Correlation with the Guide Star Catalog ^{*}

S. Vennes^{1†‡}, A. Kawka^{1†‡}, and P. Németh^{1,2†}

¹*Astronomický ústav AV ČR, Fričova 298, CZ-251 65 Ondřejov, Czech Republic*

²*Department of Physics and Space Sciences, 150 W. University Blvd, Florida Institute of Technology, Melbourne, FL 32901, USA*

ABSTRACT

We assembled a catalogue of bright, hot subdwarf and white dwarf stars extracted from a joint ultraviolet, optical, and infrared source list. The selection is secured using colour criteria that correlate well with effective temperatures $T_{\text{eff}} \gtrsim 12,000$ K. We built a $N_{\text{UV}} - V$ versus $V - J$ diagram for $\gtrsim 60,000$ bright sources using the *Galaxy Evolution Explorer* (*GALEX*) N_{UV} magnitude ($N_{\text{UV}} < 14$), and the associated Guide Star Catalog (GSC2.3.2) photographic quick- V magnitude and the Two Micron All Sky Survey (2MASS) J and H magnitudes. This distillation process delivered a catalogue of ≈ 700 sources with $N_{\text{UV}} - V < 0.5$ comprising ~ 160 known hot subdwarf stars and another ~ 60 known white dwarf stars. A reduced proper-motion diagram built using the proper-motion measurements extracted from the Naval Observatory Merged Astrometric Dataset allowed us to identify an additional ~ 120 new hot subdwarf candidates and ~ 10 hot white dwarf candidates. We present a spectroscopic study of a subset of 52 subdwarfs, 48 of them analysed here for the first time, and with nine objects brighter than $V \sim 12$. Our sample of spectroscopically confirmed hot subdwarfs comprises ten sdO stars and 42 sdB stars suitable for pulsation and binary studies. We also present a study of 50 known white dwarfs selected in the *GALEX* survey and six new white dwarfs from our catalogue of subluminous candidates. Ultraviolet, optical, and infrared synthetic magnitudes employed in the selection and analysis of white dwarf stars are listed in appendix.

Key words: stars: fundamental parameters – subdwarfs – ultraviolet: stars – white dwarfs

1 INTRODUCTION

Surveys of blue- or ultraviolet (UV)-excess objects are a rich source of hot subluminous stars and are beneficial to the study of hot subdwarf and white dwarf stars. Following the pioneering work of Humason & Zwicky (1947), colourimetric surveys, such as the northern and southern Tonantzintla survey (TON/TON-S, see Iriarte & Chavira 1957) and the Palomar-Haro-Luyten survey (Haro & Luyten 1962) provided for many years the source lists for spectroscopic observations and analysis of faint blue stars at high-Galactic latitude (e.g., Greenstein 1966; Greenstein & Sargent 1974).

The spectroscopic observation and spectral classification of samples of subluminous stars (e.g., Humason & Zwicky 1947; Feige 1958; Cowley 1958; Slettebak, Bahner, & Stock 1961; Berger 1963) helped Greenstein & Sargent (1974) define the extended (or extreme) horizontal branch (EHB) in the HR diagram. Their diagram comprising 189 faint blue stars shows a sequence of hot white dwarfs ranging from $T_{\text{eff}} \approx 14,000$ to 56,000 K and overlapping with a sequence of sdO stars in the higher range of temperatures and luminosities ($\log L/L_{\odot} \gtrsim 0$). The evolutionary tracks of Paczyński (1971a,b) suggested for the first time that helium stars with masses in the range $0.5 - 0.85 M_{\odot}$ and without hydrogen envelopes evolve from the EHB toward the white dwarf cooling sequence. However, based on EHB space density and birthrate estimates, Heber (1986) concluded that the EHB channel contributes only a small percentage of objects on the white dwarf cooling sequence with the majority following the channel connecting planetary nebula nuclei to the white dwarfs (Drilling & Schoenberner 1985).

Greenstein & Sargent (1974) also found that most EHB

^{*} Based on observations made with ESO telescopes at the La Silla Paranal Observatory under programmes 82.D-0750, 83.D-0540, and 085.D-0866.

[†] E-mail: vennes@sunstel.asu.cas.cz (SV); kawka@sunstel.asu.cas.cz (AK); nemeth@sunstel.asu.cas.cz (PN)

[‡] Visiting Astronomer, Kitt Peak National Observatory, National Optical Astronomy Observatory, which is operated by the Association of Universities for Research in Astronomy (AURA) under cooperative agreement with the National Science Foundation.

stars have weak helium and weak heavy element lines, hence the label population II or “halo”, and are classified as sdB stars in contrast with the helium-rich sdO stars. In addition, the luminosity-to-mass ratio L/M , or its reciprocal $g\theta^4$ (where $\theta = 5040 K/T_{\text{eff}}$), appeared approximately constant among these objects. Applying a model atmosphere analysis to their sample, Greenstein & Sargent extracted temperature (T_{eff}) and surface gravity ($\log g$) measurements and, since $L/M \propto T_{\text{eff}}^4/g$, they estimated $L/M \approx 68 L_{\odot}/M_{\odot}$, or $L = 46 L_{\odot}$ for a representative mass of $\approx 0.66 M_{\odot}$. The amount of hydrogen present in the star was unknown although they surmised that the nearly constant luminosity-to-mass ratio implied a thin hydrogen envelope.

The ground-based blue-excess surveys were soon followed by space-borne UV surveys. The TD-1 satellite conducted a systematic, all-sky survey (Thompson et al. 1978; Carnochan & Wilson 1983) that included the Galactic plane. The survey was conducted in four bands, one photometric band centred on 2700 Å and three low-resolution spectroscopic bands centred on 1565, 1965, and 2365 Å. The original catalogue of Thompson et al. (1978) includes 31215 entries with the catalogue prefix “TD1”, out of which Carnochan & Wilson (1983) listed 464 objects with UV colours of spectral types B4V or earlier. Among these objects, 47 were labelled as subdwarfs (“sd”). The spectroscopic identifications were secured optically. For example, Berger & Fringant (1980) listed 28 hot subluminous stars, thirteen of them new objects listed with the “UVO” catalogue prefix.

The sdB and sdO stars detected in the TD-1 have visual magnitudes ranging from 8 to 12 and are, to this day, the brightest stars of their class. For example, the brightest star in the sample is the sdO HD 49798 (Jaschek & Jaschek 1963; Mereghetti et al. 2009) with a UV flux at 2740 Å of $f_{\lambda} = 1.6 \times 10^{-11} \text{ erg cm}^{-2} \text{ s}^{-1} \text{ Å}^{-1}$, or $m_{\text{AB}}(2300\text{Å}) = 7.8 \text{ mag}$ in the AB magnitude system¹. The next two brightest evolved stars are HD 76431 (Berger & Fringant 1980; Ramspeck, Heber, & Edelmann 2001) and BD+75 325 (Gould, Herbig, & Morgan 1957) with $m_{\text{AB}}(2300\text{Å}) = 8.9 \text{ mag}$. Few hot white dwarfs like UVO2309+10 (=BPM 97895, GD 246; Luyten 1963; Giclas, Burnham, & Thomas 1965) were originally listed by Carnochan & Wilson (1983), but TD-1 UV photometry eventually led to discoveries such as the white dwarf companions to the F7 II star HR 3643 and the F4 V star 56 Persei (Landsman, Simon, & Bergeron 1996). In summary, the TD-1 UV catalogue includes objects with $m_{\text{AB}}(2300\text{Å}) \leq 11.5 \text{ mag}$, and, after early-type main-sequence stars, it is populated mostly with hot sdB and sdO stars.

Furthermore, the Orbiting Astronomical Observatory-2 (OAO-2, Code, Holm, & Bottemiller 1980) delivered a catalogue of 531 pointed UV sources that contained few white dwarfs (e.g., Feige24, Holm 1976) and ≈ 20 hot subdwarfs. The Astronomical Netherlands Satellite (ANS) also produced a catalogue of 3573 pointed UV sources (Wesselius et al. 1982) listing ≈ 10 hot white dwarfs, analysed by Wesselius & Koester (1978), and about three times as many hot subdwarfs. These experiments pre-selected bright subdwarfs with $f_{\lambda} \gtrsim 10^{-13}$ and 4×10^{-14}

$\text{erg cm}^{-2} \text{ s}^{-1} \text{ Å}^{-1}$ corresponding to $m_{\text{AB}}(2300\text{Å}) \lesssim 13.4$ and $\lesssim 14.4$, respectively. Although the OAO-2 and ANS reached fainter magnitudes, the all-sky coverage of the TD-1 survey allowed for the systematic identification of new subluminous stars. Ultraviolet flux measurements of subluminous stars are also listed in the Midcourse Space Experiment (MSX) UV catalogue (Newcomer et al. 2004).

Large catalogues of subluminous stars were first built based on extensive blue and UV-excess surveys such as the Palomar-Green (PG) survey (Green, Schmidt, & Liebert 1986), the Kitt-Peak-Downes (KPD) survey (Downes 1986), the Edinburgh-Cape (EC) survey (Kilkenny et al. 1997), the Montreal-Cambridge-Tololo (MCT) survey (Lamontagne et al. 2000), or the First Byurakan Survey (FBS, Mickaelian 2008). These and similar catalogues provided the basis for our current understanding of EHB and post-EHB stars, as well as post-asymptotic giant branch (AGB) stars.

Detailed spectroscopic studies based on the PG survey (Moehler, Heber, & de Boer 1990a; Saffer et al. 1994) placed hot sdB stars in the $T_{\text{eff}} - \log g$ diagram close to the evolution tracks of Caloi (1989) for core helium-burning stars with very thin hydrogen envelopes and masses near $0.5 M_{\odot}$. Recent spectroscopic investigations of the Hamburg-Schmidt (HS) subdwarf catalogue (Edelmann et al. 2003) using the evolutionary models of Dorman, Rood, & O’Connell (1993) confirmed the basic picture. High mass-loss rates are possibly responsible for thinning the hydrogen envelope and preventing the star from climbing the asymptotic giant branch (D’Cruz et al. 1996). Other formation scenarios examined by Han et al. (2002, 2003) involve a common-envelope phase or an episode of Roche lobe overflow that may help remove the hydrogen envelope and direct the star toward the EHB as originally proposed by Mengel et al. (1976), or involve the merger of two helium white dwarfs. Indeed, Maxted et al. (2001), Morales-Rueda et al. (2003), and Edelmann et al. (2005) found that a significant fraction of these stars reside in spectroscopic binary systems in support of the scenario for the formation of sdB stars through close binary evolution.

The evolutionary paths leading to the formation of helium rich subdwarfs (sdO) are less certain although the helium double-degenerate mergers (Han et al. 2002, 2003) or helium flash/mixing (Sweigart, Mengel, & Demarque 1974; Sweigart 1997a,b) may account for the paucity of hydrogen. Analysis of helium-rich subdwarfs (sdO) from the PG survey (Dreizler et al. 1990; Thejll et al. 1994) suggest that sdO stars evolved away from the EHB. Recently, Stroerer et al. (2007) draws further distinction between helium-deficient sdO stars and helium-enriched sdO stars, with the former linked to sdB stars and the latter possibly formed in the merger of helium white dwarfs, or via helium mixing. Detailed abundance studies (e.g., Lanz et al. 2004; Ahmad et al. 2007) offers insights into the formation of helium-rich subdwarf stars involving helium mixing. Based on a population study Zhang, Chen, & Han (2009) conclude that many sdO stars evolve directly from sdB stars, and that only the more massive sdO stars ($M > 0.5 M_{\odot}$) are the outcome of white dwarf mergers.

The majority of white dwarfs are formed through the post-AGB channels (Drilling & Schoenberner 1985; Heber 1986). Initial estimates of the death-rate of main-

¹ $m_{\text{AB}} = -2.5 \log f_{\nu} - 48.6$.

sequence stars and of the birth-rate of white dwarf stars show broad agreement between the rates although they were still affected by considerable uncertainties (see Drilling & Schoenberner 1985). Post-AGB stars are powered by a hydrogen-burning shell in thermal equilibrium interspersed with thermal pulses (helium-shell flash). The evolutionary tracks of Schoenberner (1983) connect the AGB stars to the white dwarfs by invoking a phase of enhanced mass-loss (or super-wind) that occurs between pulses, i.e., during the hydrogen shell-burning phase. Higher mass-loss rates imply shorter evolutionary time-scales and, therefore, the assumed rates affect the growth of the carbon/oxygen core and determine the final mass of the nascent white dwarf. Weidemann (2000) compared available data to the results of model calculations (e.g., Vassiliadis & Wood 1993) linking the initial main-sequence mass to the final white dwarf mass. Observations of white dwarfs in stellar systems where evolutionary time-scales are measurable, i.e., clusters (e.g., Kalirai et al. 2008) or evolved binaries, provide the data and constrain the initial-mass to final-mass problem (Weidemann 2000). Properties of white dwarfs in spectroscopic and colourimetric studies are parametrized by T_{eff} and $\log g$ that are transformed into ages (t_{cool}) and masses (M/M_{\odot}), hence radii (R/R_{\odot}), using evolutionary models (e.g., Wood 1995; Benvenuto & Althaus 1999).

Extensive colourimetric surveys such as the PG survey helped establish the character of the white dwarf population such as its local space density and formation rate (Green 1980; Liebert, Bergeron, & Holberg 2005) while deeper surveys such as the Two-Degree Field (2dF) survey allowed to probe the spatial distribution of the white dwarf population and determine its Galactic scale-height (Vennes et al. 2002). Deep and extensive colourimetric surveys such as the Sloan Digital Sky Survey (SDSS, e.g., Eisenstein et al. 2006) and, potentially, Galaxy Evolution Explorer (GALEX) all-sky survey combined with kinematical data (e.g., Salim & Gould 2003; Lépine & Shara 2005) should help retrace the Galactic history, i.e., birth rates and time scales, of the white dwarf population.

We have initiated a program aimed at identifying the white dwarf population in the GALEX all-sky survey. As a first instalment, we present a new sample of bright subluminous stars based on GALEX and matched with optical/infrared source catalogues (Section 2). The sample is particularly suitable for GAIA Calibration (Soubiran et al. 2008) and adds material for surveys of pulsating, hot subdwarfs (Billères et al. 2002; Østensen et al. 2010). We describe the source selection in Section 2.1, the spectroscopic follow-up in Section 2.2, and the model atmospheres employed in the analysis in Section 2.3. Next, we present the bright ($V < 12$) catalogue in Section 3.1 and a model atmosphere analysis of the new subdwarfs and white dwarfs in sections 3.2 and 3.3, respectively. We conclude in Section 4. Photometric ultraviolet, optical, and infrared absolute magnitudes, suitable for the study of hot white dwarfs in multiwavelength surveys, are listed in Appendix A.

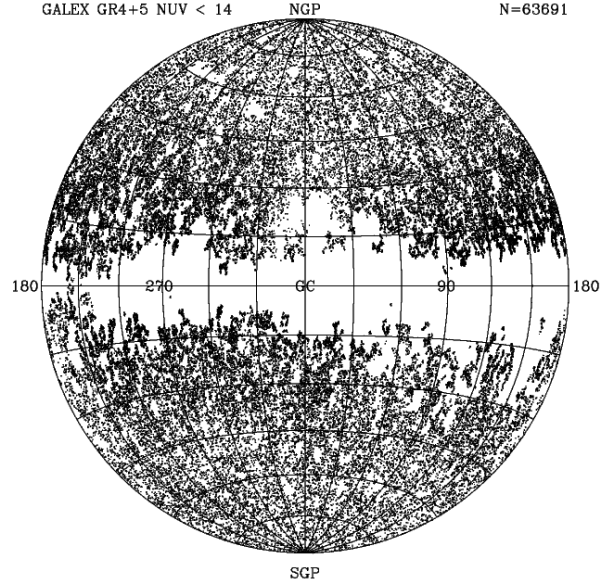


Figure 1. Distribution of the GALEX/GSC selection in Galactic coordinates. The selection of 63691 stars with GALEX $N_{\text{UV}} < 14$ mag is restricted to Galactic latitudes $|b| \gtrsim 10\text{-}20^\circ$ and occupies an area of 25000 square degrees.

2 A GALEX/GSC SURVEY

2.1 Source selection

We obtained UV photometry from the Galaxy Evolution Explorer (GALEX) all-sky survey. GALEX provides photometry in two bands, F_{UV} and N_{UV} . The F_{UV} bandpass is $1344 - 1786 \text{ \AA}$ (defined at $\gtrsim 10\%$ peak value) with an effective wavelength of 1539 \AA , and the N_{UV} bandpass is $1771 - 2831 \text{ \AA}$ with an effective wavelength of 2316 \AA (see Morrissey et al. 2007). We searched the GALEX GR4+5 release using the CasJobs batch query services with the following criteria:

$$N_{\text{UV}} \leq 14, \quad N_{\text{UV}} \geq 0, \quad F_{\text{UV}} \geq 0,$$

and we extracted the parameters ra , dec , nuv_mag , nuv_magerr , fuv_mag , fuv_magerr , fov_radius , and e_bv . The right ascension and declination (ra , dec) supplied by GALEX are J2000. The N_{UV} and F_{UV} magnitudes (nuv_mag , fuv_mag) and associated errors (nuv_magerr , fuv_magerr) are defined in the AB system. We opted for magnitudes calculated using the SExtractor “mag_auto” with a variable elliptical aperture rather than a fixed aperture. The distance of the source from the image (or tile) centre (foc_radius) is measured in degrees, and each tile has a field of view of 1.25° in the N_{UV} or 1.27° in the F_{UV} . Finally, the total extinction in the line-of-sight (e_bv) is based on the maps of Schlegel, Finkbeiner, & Davis (1998). However, reddening corrections were not initially applied because we lack a priori knowledge of the distance and spectral type.

A selection of bright stars with GALEX suffers potential photometric inaccuracies. First, the imaging quality degrades toward the edge of the tile (Morrissey et al. 2007) altering the point spread function (PSF). Next, the corrections for photometric nonlinearity are uncertain and depend on the aperture size. This effect, compounded with

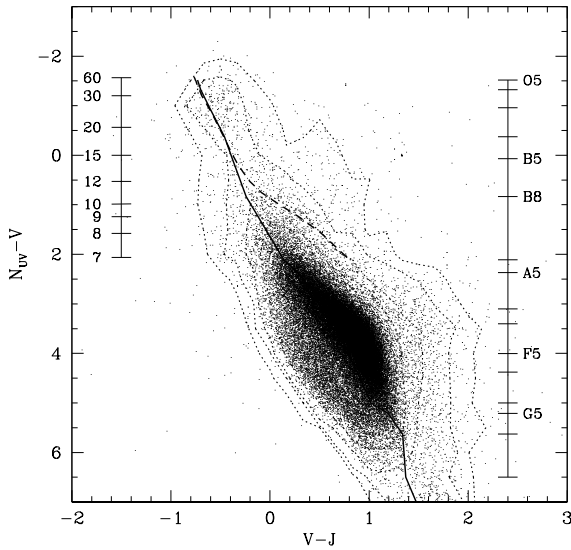


Figure 2. Colour indices ($N_{UV} - V$ versus $V - J$) of 60379 stars from the joint *GALEX/GSC* survey. The locations of the main-sequence (full line) and white dwarf cooling sequence (dashed line, $\log g = 8$) are shown. Contour lines (dotted lines) show the number density of stars (per square magnitude) at 1%, 3%, 10%, and 30% of the peak density. The corresponding white dwarf temperature scale is shown on the left, and the main sequence spectral types on the right. No corrections are applied for interstellar reddening.

the broadening of the PSF for off-centre sources, introduces a systematic offset between predicted and measured magnitudes. In practice, we applied the nonlinearity correction for a $3'$ aperture and labelled as potentially inaccurate the photometry of sources located more than 0.4° from the tile centre. The requirement that the F_{UV} detection be included could also result in many bright objects being dropped from the list. A N_{UV} -only selection that may potentially triple the membership to the bright source list will be examined elsewhere.

Entries with coordinates matching within 10^{-3} degrees were merged and the search resulted in the selection of $N = 63691$ individual sources. Figure 1 shows the source locations in Galactic coordinates. The GR4+5 release covers ~ 25000 square degrees and excludes the Galactic plane.

Next, we cross-correlated the source list with the Guide Star Catalog version 2.3.2 (GSC2.3.2, Lasker et al. 2008) using VizieR at the Centre de Données astronomiques de Strasbourg². The closest GSC entry found within a radius of 10 arcseconds of the *GALEX* coordinates is thereby associated with the UV source. The joint *GALEX/GSC* survey comprises $N = 60204$ sources, or 96% of the total, in the $3''$ sample and $N = 62672$ sources in the $10''$ sample. For each object we recorded both UV magnitudes (F_{UV} , N_{UV}) and we adopted the “quick- V ” (V_{12}) magnitude which is close to the Johnson V magnitude, $V_{12} = V - 0.15(B - V)$

(Russell et al. 1990). Following the same positional criteria we also obtained the infrared photometry from the Two Micron All Sky Survey (2MASS; Skrutskie et al. 2006), which is available at VizieR on CDS.

Figure 2 shows a $N_{UV} - V$ versus $V - J$ diagram of our *GALEX/GSC* selection. The data are compared to synthetic main-sequence and white dwarf colours. The procedure selects objects with temperatures above 12,000 K, or spectral types earlier than $\sim B8$.

Finally, we built a sample of $N = 694$ UV-excess objects by restricting the index $N_{UV} - V < 0.5$. The choice of the $N_{UV} - V$ index as a primary selection criterion is motivated by the need to mitigate the effect of binary companions on the selection of white dwarf stars. Although the 2MASS J magnitude is generally more reliable than the GSC V_{12} magnitude it is potentially contaminated by a putative main-sequence companion to the target white dwarf star (see Section 3.3).

We obtained proper-motion for each object from the Naval Observatory Merged Astrometric Dataset (NOMAD Zacharias et al. 2004) accessed at VizieR. Then, we calculated the reduced proper-motion index H :

$$H = V + 5 \log \mu + 5 = M_V + 5 \log v_T - 3.3791,$$

where μ is the proper-motion in units of arcsecond yr^{-1} , and v_T is the transverse velocity in km s^{-1} . Figure 3 shows the index H versus the colour index $N_{UV} - V$ for the sample of 694 objects with, on the left panel, the subset of known subdwarfs marked, and, on the right, the known white dwarfs also marked. A white dwarf sequence at $0.6 M_\odot$ (see Appendix A) is drawn covering the temperature between $T_{\text{eff}} = 12000$ and 84000 K at three representative transverse velocities. Figure 4 shows the corresponding H distribution functions for the known white dwarfs and subdwarfs. Hot white dwarfs dominate the number count at $H \gtrsim 13$ while hot subdwarfs are predominant in the range $H \lesssim 12$. The H distribution functions are converted into a transverse velocity distribution by calculating the absolute V magnitude M_V for each object and solving for the velocity.

Greenstein & Sargent (1974) already suggested that stars on the EHB have similar luminosities. Based on $g\theta^4$ values of 2.35 (Greenstein & Sargent 1974), 2.28 (Moehler, Heber, & de Boer 1990a)³, 2.64 (Saffer et al. 1994), and 2.73 from the population synthesis of Han et al. (2003), we adopted a mean $\bar{M}_V \approx 4.2 \pm 0.5$ for the subdwarfs. We found that the transverse velocities follow a distribution of the form $N \propto e^{-v_T/\sigma_v}$ with $\sigma_v \approx 60 \text{ km s}^{-1}$. Based on a similar sample of hot subdwarf stars, Thejll et al. (1997) concluded that these objects belong to the old thick Galactic disc. Similarly, Altmann, Edelmann, & de Boer (2004) found that 87% of their sample of sdB stars belong to the thick disc with the remainder in the Galactic halo.

Next, we estimated M_V for each white dwarf by adopting a mean mass of $0.6 M_\odot$ and by estimating T_{eff} using the $N_{UV} - V$ colour index. We used the mass-radius relations of

² CDS available at <http://cdsweb.u-strasbg.fr/CDS.html> (Ochsenbein, Bauer, & Marcout 2000).

³ Edelmann et al. (2003) state that the Strömgren calibration used by Moehler, Heber, & de Boer (1990a) may have been inappropriate for sdB stars which may explain their lower mean value for $g\theta^4$. Nonetheless, we include the value in the average and account for the possible uncertainties.

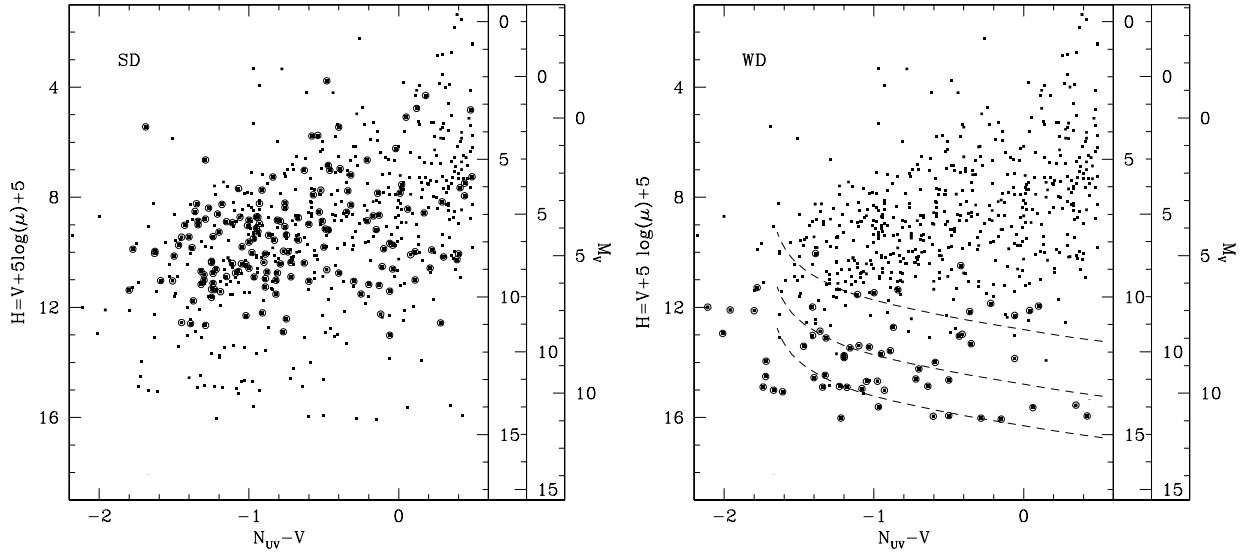


Figure 3. Reduced proper-motion diagram of a sample of $N = 694$ UV-excess objects with $N_{UV} - V < 0.5$. The scales on the right-hand side show the corresponding absolute V magnitudes for transverse velocities of, from inside to outside, 10, 25, and 50 km s^{-1} . The samples of known hot subdwarfs (left) and white dwarfs (right) are shown with open circles and comprise 159 and 61 objects, respectively. The white dwarf sequence at $0.6 M_{\odot}$ (dashed lines) is shown for tangential velocities of, from top to bottom, 10, 25, and 50 km s^{-1} . No corrections are applied for interstellar reddening.

Wood (1995) and Benvenuto & Althaus (1999). The resulting white dwarf velocities follow the same relation but with $\sigma_v \approx 40 \text{ km s}^{-1}$. The kinematics of hot white dwarfs also suggest that they belong to the old disc (Sion et al. 1988).

The apparent deficit in blue ($N_{UV} - V \lesssim -0.5$), luminous ($H \lesssim 6$) stars in the upper-left corner of Figure 3 is caused in part by interstellar extinction affecting more distant stars and in part by the relative rarity of luminous blue stars. Using the $R_V = 3.2$ parametrization of Cardelli, Clayton, & Mathis (1989), we estimate $A_{N_{UV}}/E_{B-V} = 7.75$ while $A_V/E_{B-V} = 3.2$. For a hypothetical, distant star with $E_{B-V} = 0.2$, the ultraviolet-optical colour correction would be $(N_{UV} - V) - (N_{UV} - V)_0 = +0.91$. The corresponding shift in colour would displace an intrinsically blue object in Figure 3 close to a magnitude toward the right. This effect, not apparent at lower luminosities, helps draw further distinctions between luminous and subluminous stars that are not affected to the same degree by interstellar extinction.

The information gathered from the sample of known objects is useful in distinguishing the white dwarf and subdwarf populations based on the observed H distribution.

2.2 Follow-up optical spectroscopy

We obtained low dispersion spectra of subluminous candidates using the EFOSC2 (ESO Faint Object Spectrograph and Camera) attached to the New Technology Telescope (NTT) at La Silla Observatory, and using the RC Spectrograph (Ritchey-Chretien Focus Spectrograph) attached to the 4-m telescope at Kitt Peak National Observatory (KPNO).

At the NTT on UT 2008 October 19-22, 2009 March 2-

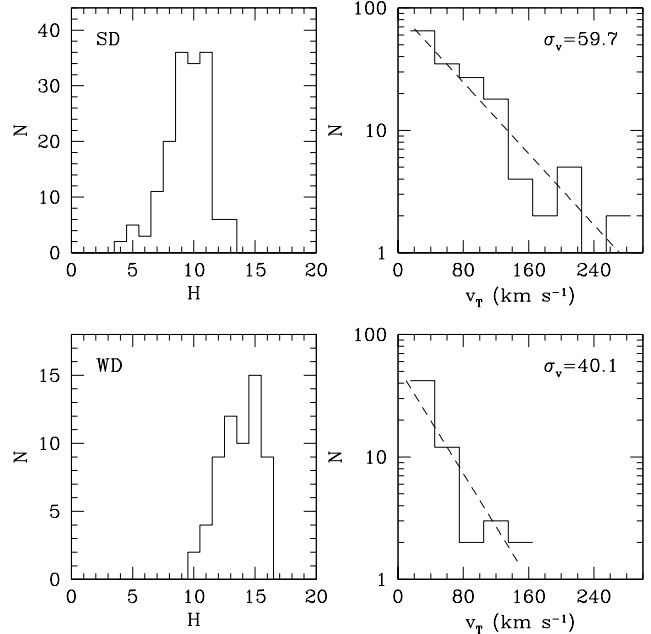


Figure 4. Distribution of H (left) and corresponding transverse velocities v_T (right) for hot subdwarfs (top) and white dwarfs (bottom). The velocity distribution functions follow $N \propto e^{-v_T/\sigma_v}$, with the best-fit values given in the upper right corner above the distributions.

4, and 2009 August 23-27 we employed the grism #11 (300 lines per mm) with a dispersion of $\approx 4.17 \text{ \AA}$ per binned pixel (2×2). The slit width was set at $1''$ resulting in a resolution of $\approx 16 \text{ \AA}$. At the NTT on UT 2010 March 2-4 we employed

grism #7 (600 lines per mm) with a dispersion of $\approx 1.96 \text{ \AA}$ per pixel. The slit width was set at $1''$ resulting in a resolution of $\approx 8 \text{ \AA}$. Finally, at KPNO on UT 2010 March 23-26 we employed the KPC-10A grating (316 lines per mm) with a dispersion of 2.75 \AA per pixel in first order and centred on 5300 \AA . The slit width was set at $1.5''$ resulting in a spectral resolution of $\approx 5.5 \text{ \AA}$.

Our spectroscopic observations are progressing toward decreasing H values. The sample $H \geq 13$ is completed and the sample with $H \geq 11$ is 80% completed. We obtained high signal-to-noise spectra suitable for detailed line profile analysis. This analysis is based on the calculation of model grids and detailed synthetic hydrogen and helium line profiles.

2.3 Model atmospheres

We computed a grid of high-gravity models in local thermodynamic equilibrium (LTE) suitable for the analysis of hydrogen-rich white dwarfs. The models are in convective/radiative equilibrium and assume plane parallel geometry. The model opacities include hydrogen bound-bound, bound-free, and free-free absorptions, as well as H^- bound-free and free-free absorptions at lower temperatures. The model opacities also include the hydrogen Rayleigh scattering and the electron scattering. The grid covers a range of parameters suitable for the analysis of hydrogen-rich white dwarfs with T_{eff} from 7000 to 100000 K, $\log g$ from 5.5 to 9.5, and a pure hydrogen composition. Detailed hydrogen line profiles are computed using the tables of Lemke (1997). Kawka & Vennes (2006) provide additional details of the model calculations⁴. We describe in Appendix A and employ in Section 3.3 a set of absolute magnitudes computed using these white dwarf models.

Next, we computed a grid of non-LTE model atmospheres and synthetic spectra covering a range of parameters (T_{eff} , $\log g$, $\log n(\text{He})/n(\text{H})$) suitable for hydrogen and helium-rich subdwarf stars using the codes TLUSTY-SYNPEC (Hubeny & Lanz 1995; Lanz & Hubeny 1995). The models are regrouped in three overlapping grids with grid number 1 suitable for sdB stars covering T_{eff} from 21000 to 35000 in steps of 1000 K, $\log g$ from 4.5 to 6.25 in steps of 0.25 dex, and $\log n(\text{He})/n(\text{H})$ from -4 to -1 in steps of 0.5 dex. Similarly, grid number 2, suitable for sdB and sdO stars, covers T_{eff} from 25000 to 45000, $\log g$ from 5.0 to 6.25, and $\log n(\text{He})/n(\text{H})$ from -3 to 0. Finally, grid number 3, suitable for helium-rich stars, covers T_{eff} from 34000 to 60000 in steps of 2000 K, $\log g$ from 5.0 to 6.25, and $\log n(\text{He})/n(\text{H})$ from 0 to 2. The hydrogen, neutral helium, and ionized helium models comprise 9, 24, and 20 energy levels, respectively. Figure 5 shows model spectra representative of the sdB and sdO classes.

⁴ Recent improvements in hydrogen line broadening theory taking into account non-ideal effects (Tremblay & Bergeron 2009) could result in upward revisions of our T_{eff} and $\log g$ measurements by up to 10% and 0.15 dex, respectively.

3 A CATALOGUE OF SUBLUMINOUS STARS

3.1 Sample of bright ($V < 12$) sublumino- candidates

The bright selection potentially harbours new nearby subdwarf or white dwarf stars. Table 1 lists bright UV-selected stars ($V < 12$) showing the predominance of massive B stars, followed by hot subdwarfs (sdO, sdB), white dwarfs (DN=dwarf nova, PNN=planetary nebula nucleus, DA), and a nova-like star (NL). The content of this list resembles and complements the TD-1 catalogue of UV-bright stars. Only about 10% of UV sources listed by Carnochan & Wilson (1983) are sublumino stars, compared to $\approx 30\%$ in Table 1. The N_{UV} magnitudes range from 10.5 to 12.5 while $m_{\text{AB}}(2300\text{\AA}) \leq 11.5$ in the TD-1 survey, suggesting, as expected, that sublumino stars should dominate fainter selections such as the present *GALEX* selection.

The bright source list includes a single white dwarf, G191-B2B, and 15 hot subdwarfs. No new white dwarfs were found in the bright source list. Six of the subdwarfs were previously known: the hot sdO stars Feige 67 and Feige 110, the He-sdB star CPD-20 1123 (Albus 1), the TD-1 discovery UVO 0825+15, the sdB plus GV binary EC 11031-1348, and the pulsating sdB EC 20117-4014 (O'Donoghue et al 1997). An additional nine new subdwarfs complete the bright source list, including the newly identified binaries *GALEX* J0321+4727 and *GALEX* J2349+3844 (Kawka et al. 2010a). The sdB *GALEX* J0321+4727 is in a 0.26584 d binary with a late-type companion showing a large reflection effect, while the sdB *GALEX* J2349+3844 is in a 0.46249 d binary with, most probably, a white dwarf companion. The brightest new subdwarf in our sample is CD-32 1567 with $V = 11.2$.

Samples of bright, nearby white dwarfs are largely based on the Lowell proper-motion survey (Giclas, Burnham, & Thomas 1980), listed with the GD and GR prefixes, or the New Luyten Two-Tenth survey (Luyten 1979, 1980; Salim & Gould 2003), listed with the NLTT prefix. Of the ten known white dwarfs brighter than $V = 12$, only RE 2214-492 is a relatively recent discovery (Holberg et al. 1993) in the ROSAT/Wide Field Camera extreme-UV survey (see Mason et al. 1995). Based on their expected UV flux output, eight out of the ten known white dwarfs brighter than $V = 12$ were eligible for detection, while the remaining two objects (WD 1142-645 and WD 0839-327) have low UV flux output. However, the fields surrounding WD 1142-645, WD 0839-327, Procyon B (WD 0736+053), Sirius B (WD 0642-166), WD 2032+248 (Wolf 1346), and WD 1620-391 (CD-38 10980) are close to the Galactic plane in areas not covered in the *GALEX* survey. Three of the remaining objects suffered various defects mainly caused by their excessive UV brightness: WD 0413-077 (40 Eri B) is in fact not included in GSC2.3.2 although it would still have been excluded from our selection because of the poor quality of the N_{UV} and F_{UV} photometry; WD 0310-688 was also excluded because of the unreliability of the N_{UV} photometry; RE 2214-492 was excluded from our selection because of the lack of F_{UV} photometry. Because it met all the criteria, WD 0505+527 (G191-B2B) is the only white dwarf retrieved in the bright source list.

Table 1. Sample of bright ($V < 12$) subluminous candidates.

RA (J2000)	Dec (J2000)	N_{UV} (mag)	V_{12} (mag)	μ^a (mas yr $^{-1}$)	Name	Type	Telescope
0 13 01.0	+72 31 19	11.97	11.49	9.3 ± 6.3	NGC 40	PNN	...
2 10 22.9	+29 27 27	12.32	11.91	6.6 ± 0.9	uvby98 610242080	B	3.58m
2 45 24.7	+32 45 29	11.45	11.33	3.6 ± 0.8	TYC 2329-941-1	B	3.58m
2 45 56.8	+11 50 15	11.55	11.87	9.2 ± 2.9	...	B	3.58m
3 15 08.3	+14 53 49	11.45	10.97	5.9 ± 3.3	US 3783,HIP 15137	B ^b	3.58m
3 21 39.8	+47 27 17	11.91	11.70	59.5 ± 0.7	Cl Melotte 20 488	sdB ^c	4.0m
4 01 05.4	-32 23 48	11.03	11.20	31.3 ± 1.7	CD-32 1567	sdB	3.58m
4 24 41.2	-20 07 12	12.13	11.92	57.9 ± 3.7	IM Eri	NL	...
4 47 04.2	-67 06 52	11.61	11.26	< 4.3	HD 270754	B1.5Ia ^d	...
5 05 30.7	+52 49 50	10.63	11.74	90.9 ± 2.4	G191-B2B	DA WD ^e	...
6 06 13.3	-20 21 07	11.81	11.80	16.2 ± 4.0	CPD-20 1123, Albus 1	He-sdB ^f	...
6 36 46.5	+47 00 25	11.91	11.88	2.5 ± 1.0	...	B	4.0m
6 39 21.4	+33 23 52	11.77	11.63	5.6 ± 1.3	...	B	4.0m
6 39 52.1	+51 56 58	12.47	11.99	37.5 ± 3.1	...	sdB	4.0m
6 57 36.8	-73 24 47	10.99	11.90	114.8 ± 1.9	CPD-73 420	sdB	3.58m
7 02 22.2	+18 40 32	12.29	11.98	< 5.0	...	B	3.58m
7 37 25.2	+37 14 01	10.57	10.81	6.1 ± 1.3	KUV 07341+3721,TD1 31205	B ^b	4.0m
7 47 21.9	+62 25 42	11.67	11.91	< 9.8	FBS 0742+625	sdB	4.0m
8 08 37.6	+29 08 40	11.90	11.44	12.1 ± 1.8	TYC 1939-499-1	A	4.0m
8 25 13.5	+73 06 38	12.27	11.78	19.7 ± 2.8	Z Cam	DN	...
8 28 32.9	+14 52 05	11.65	11.78	23.7 ± 1.2	TD1 31206,UVO 0825+15	He-sdB ^g	3.58m
8 41 38.5	-07 26 02	12.08	11.82	< 5.6	TYC 4875-465-1	B	3.58m
9 23 00.2	-67 53 14	11.49	11.27	< 11.5	TYC 9196-1935-1	B	3.58m
10 00 59.0	+02 48 05	11.62	11.23	< 3.0	TYC 247-190-1	B	3.58m
10 35 53.2	-39 04 14	11.32	11.04	7.9 ± 2.8	TYC 7710-2503-1	B	3.58m
10 39 07.7	+36 45 33	11.23	11.25	9.9 ± 1.2	CBS 129	B ^b	4.0m
10 44 10.6	+48 19 02	12.20	11.79	14.9 ± 1.0	...	A	4.0m
11 05 41.5	-14 04 24	11.82	11.54	7.3 ± 3.0	EC 11031-1348	sdB+GV ^h	3.58m
12 11 56.5	-46 55 47	11.53	11.31	12.4 ± 1.7	...	B	3.58m
12 40 51.6	-10 54 13	11.26	10.89	< 4.2	BD-10 3529	B	3.58m
12 41 51.8	+17 31 19	10.67	11.64	37.4 ± 2.6	Feige 67,TD1 30996	sdO	...
12 45 58.8	-43 05 20	10.86	10.46	49.6 ± 2.5	CD-42 7878, HD 110942	B	3.58m
12 57 52.7	-35 27 18	11.26	11.55	9.8 ± 2.9	...	B	3.58m
13 32 59.7	-41 12 17	11.72	11.43	2.6 ± 2.1	TYC 7792-881-1	B	3.58m
13 46 47.2	-07 07 31	12.15	11.81	< 5.7	...	B	3.58m
13 48 45.0	+43 37 58	11.32	11.35	11.6 ± 2.0	FB 140	B	4.0m
14 11 16.0	-30 53 07	11.63	11.90	9.8 ± 2.4	CD-30 11223, FAUST 3993	sdB	3.58m
14 27 08.4	+72 57 50	11.51	11.21	< 19.0	...	B	4.0m
15 09 48.5	-38 44 54	11.20	10.93	3.8 ± 2.9	HD 134199,CPD-38 6054	B	3.58m
16 29 32.9	+80 16 55	11.00	10.53	< 4.9	...	B	4.0m
17 02 28.3	+63 53 31	11.58	11.99	14.1 ± 2.7	...	B	4.0m
17 23 26.6	+46 19 02	11.88	11.55	16.3 ± 2.3	TYC 3508-387-1	B	4.0m
17 36 51.3	+28 06 35	11.53	11.44	26.8 ± 0.8	TYC 2084-448-1	sdB+GV	3.58m
18 01 52.5	+37 42 09	11.72	11.37	5.4 ± 3.0	TYC 3102-1109-1	B	4.0m
18 15 13.0	+39 42 31	11.93	11.51	< 2.1	...	B	4.0m
19 11 09.3	-14 06 54	11.77	11.77	49.6 ± 4.2	...	He-sdO	3.58m
20 47 42.0	+08 46 56	11.12	10.79	5.8 ± 1.8	TYC 1089-1800-1	B	3.58m
20 15 04.8	-40 05 44	12.02	11.85	22.1 ± 2.9	EC 20117-4014	sdBV	...
23 19 58.4	-05 09 56	11.26	11.50	12.4 ± 5.2	Feige 110	sdO	...
23 49 47.8	+38 44 40	11.31	11.71	5.6 ± 0.7	FBS 2347+385	sdB ^c	2.0m

^a From NOMAD (Zacharias et al. 2004).^b The sdB classifications of Mitchell (1998), Wegner & Swanson (1990), and Wagner et al. (1988) for these objects are not confirmed.^c New subdwarfs in close binaries, see Kawka et al. (2010a).^d B1.5 Ia star in the LMC (Feast, Thackeray, & Wesselink 1960) with a B2Ia ultraviolet classification (Smith Neuhig & Bruhweiler 1999).^e DA white dwarf WD 0505+527.^f The blue star Albus 1 (Caballero & Solano 2007) was identified as a sdB-He star by Vennes, Kawka, & Smith (2007).^g Classified as a sdO by Berger & Fringant (1980).^h Reed & Stiening (2004) noted the composite optical-infrared colours.

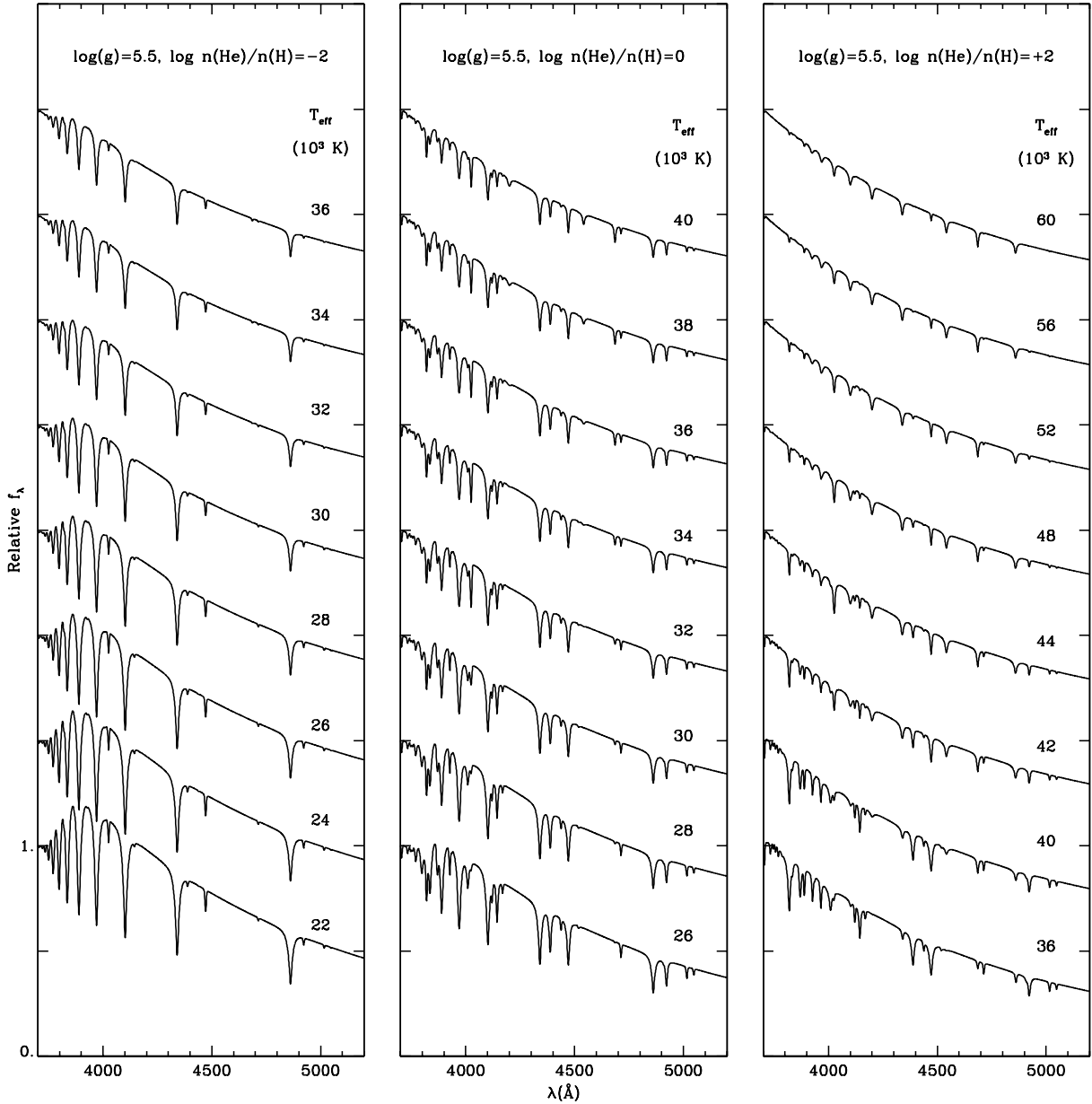


Figure 5. Model spectra for sdB stars (left panel), He-sdB stars (middle panel), and He-sdO stars (right panel) extracted from the main model grid.

3.2 Properties of the hot subdwarfs

Figure 6 shows our spectroscopy of subdwarf stars sorted by effective temperatures. Helium line strengths show large variations from one object to the next with the noteworthy cases of J0747+6225 and J0827+1753 which display strong He I line spectra. The spectra of GALEX J0934–2512 and J1632+0752 (=PG 1629+081) show peculiar He I $\lambda 4471$ /He I $\lambda 4686$ line ratios that are too weak compared to other objects with similar Balmer line spectra. The discrepancy is likely to result in helium abundance inconsistencies. Two of our targets showed composite sd+MS spectra and are not shown here (but see Section 3.2.1). Ten objects show He-rich spectra with the remainder showing H-rich spectra, or a 1:5 number ratio.

We fitted the observed spectra from H α (or H β) to H $_{11}$ with the non-LTE model grid using χ^2 minimization techniques. The quoted errors are 1- σ statistical errors. Figure 7 shows an example of an analysis of hydrogen/helium line profiles. The hot sdB star GALEX J0639+5156 is part of our bright sample ($V \sim 12$) and is typical of its class. Table 2 lists the atmospheric parameters of the hot subdwarfs observed in this program. We listed the results of our analysis for GALEX J0934–2512 and J1632+0752 excluding the He I $\lambda 4686$ line. A detailed analysis of these peculiar subdwarfs will be presented elsewhere after high-dispersion red and blue spectra are obtained. A preliminary analysis of the composite sdB+GV spectra is presented in Section 3.2.1.

The spectral classification follows a simple scheme (see

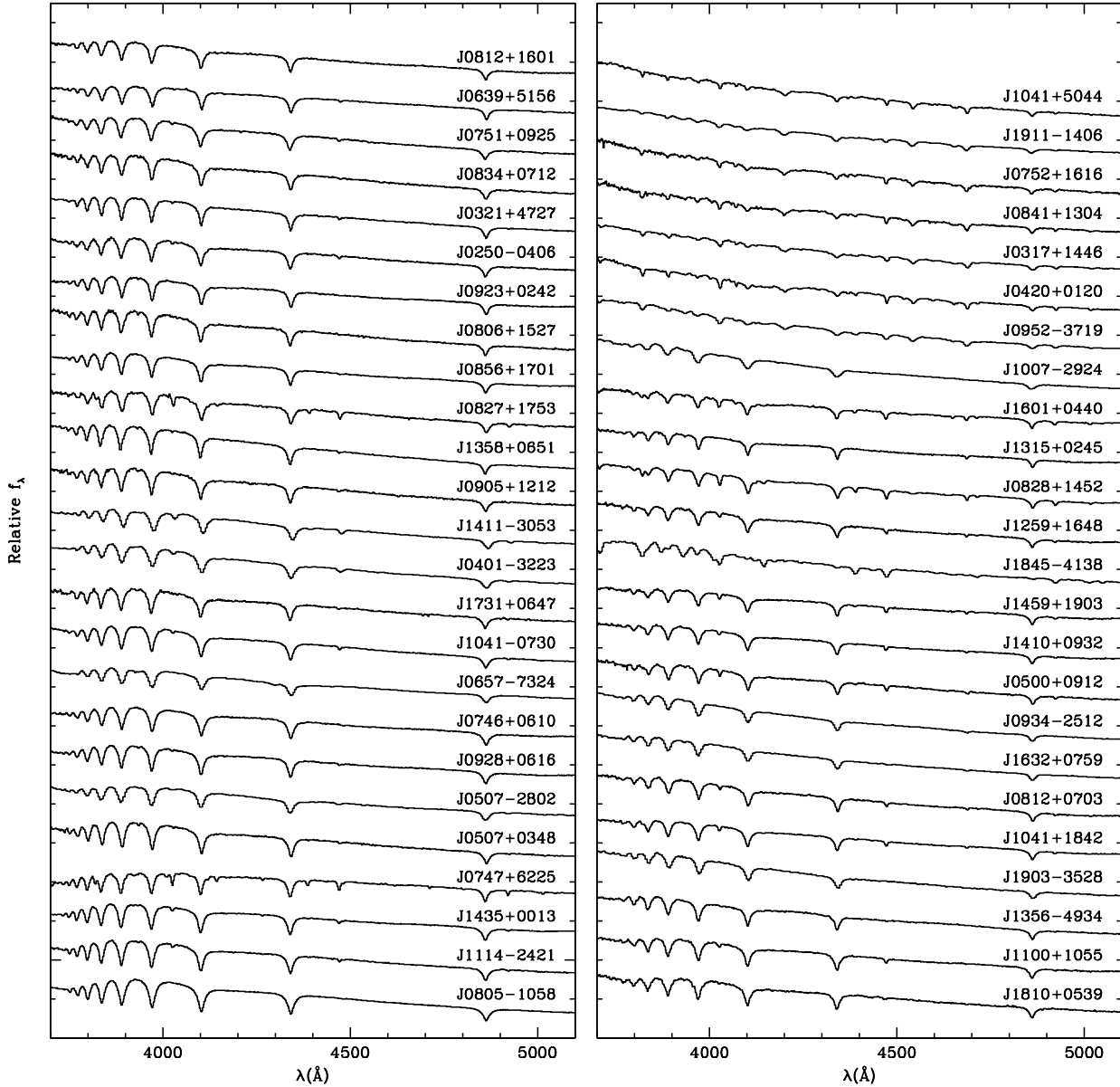


Figure 6. NTT and KPNO spectra of bright sdB and sdO stars from the *GALEX* selection ranked according to temperatures from the coolest star (lower left) to the hottest star (upper right).

a discussion in Heber 2009): spectra with dominant hydrogen Balmer lines along with weaker He I or He II lines are labelled sdB or sdO, respectively. Spectra with dominant He II lines are labelled He-sdO, whereas spectra with unusually strong He I lines are labelled He-sdB. The newly identified He-sdO *GALEX* J1911–1406 is a bright example of its class. The low-dispersion spectrum shows strong lines of the He II Pickering series, He II $\lambda 4686$, He I $\lambda 4471$, and a strong C III–IV $\lambda 4647$ – 4658 blend, and N III $\lambda 4634$ – 4641 multiplet. All He-sdO stars share these features to varying degrees and are characterized with $43000 \lesssim T_{\text{eff}} \lesssim 52000$ K, $\log g \approx 5.6$ and $\log n(\text{He})/n(\text{H}) \gtrsim 0.7$. Among their cooler counterparts, such as the He-sdB star *GALEX* J0828+1452, some have higher hydrogen abundance than He-sdO stars with

weaker carbon and nitrogen lines. Overall, our subdwarf selection displays abundance diversities often noted in sdB stars (Edelmann et al. 2003) and sdO stars (Stroeer et al. 2007).

3.2.1 The sdB+G2V binaries EC 11031–1348 and *GALEX* J1736+2806 and four binary candidates

Companions to hot subdwarf stars are often detected from radial velocity variations (Morales-Rueda et al. 2003; Kawka et al. 2010a), while more luminous companions contribute to composite spectra or colours (Aznar Cuadrado & Jeffery 2002; Stark & Wade 2003; Reed & Stiening 2004). For example, Figure 8 shows a pre-

Table 2. Properties of evolved subluminous stars.

GALEX J	Type	<i>V</i> (mag)	<i>T</i> _{eff} (K)	log <i>g</i> (c.g.s.)	log <i>n</i> (He)/ <i>n</i> (H)	Other names
025023.8–040610	sdB	13.02	28560 ± 700	5.56 ± 0.15	−2.40 ^{+0.25} _{−0.40}	HE 0247–0418, PB 9286
031737.9+144622 ^a	He-sdO	12.67	45600 ± 2300	5.81 ± 0.40	0.82 ^{+0.49} _{−0.27}	PG 0314+146
032139.8+472716 ^{b,c}	sdB	11.79	29200 ± 300	5.50 ± 0.10	−2.60 ± 0.10	
040105.3–322348 ^b	sdB	11.20	27000 ± 1300	5.36 ± 0.19	−1.63 ± 0.21	CD–32 1567
042034.8+012041	He-sdO	12.52	45000 ± 800	5.74 ± 0.15	> 1.2	
050018.9+091203	sdB	14.63	35250 ± 570	5.58 ± 0.14	−1.25 ± 0.12	
050720.3–280225	sdB	12.39	25000 ± 2500	4.90 ± 0.35	−2.20 ^{+0.40} _{−0.60}	CD–28 1974, HE 0505–2806
050735.7+034815	sdB	14.42	22050 ± 950	5.11 ± 0.16	−2.70 ^{+0.40} _{−0.75}	
063952.0+515658 ^b	sdB	11.97	30750 ± 250	5.70 ± 0.08	−2.59 ^{+0.19} _{−0.29}	
065736.8–732447 ^b	sdB	11.90	26400 ± 2000	4.79 ± 0.21	< −2.7	CPD–73 420
074617.1+061006	sdB	12.85	26100 ± 790	5.61 ± 0.15	< −3.1	
074721.9+622542 ^b	sdB	11.91	23700 ± 800	5.00 ± 0.12	−1.00 ± 0.10	FBS 0742+625
075147.0+092526	sdB	14.12	29890 ± 400	5.65 ± 0.11	−2.35 ± 0.25	
075234.2+161604	He-sdO	14.23	48750 ± 1450	5.77 ± 0.22	0.96 ^{+0.62} _{−0.26}	
080510.9–105834	sdB	12.21	21200 ± 700	5.50 ± 0.18	< −2.9	
080656.7+152718	sdB	14.69	28400 ± 950	5.26 ± 0.19	< −2.5	
081203.8+070352	sdB	14.78	34900 ± 500	5.73 ± 0.14	−1.65 ± 0.15	
081233.6+160121	sdB	13.57	30770 ± 500	5.51 ± 0.15	< −2.7	
082734.9+175358	sdB	14.62	28200 ± 850	5.30 ± 0.14	−1.04 ± 0.12	
082832.8+145205 ^b	He-sdB	11.78	36650 ± 650	5.65 ± 0.14	−0.50 ± 0.08	TD1 31206
083412.3+071211	sdB	14.86	29000 ± 600	5.46 ± 0.16	< −2.4	
084143.8+130431 ^a	He-sdO	13.66	47000 ± 1800	5.36 ± 0.27	> 0.8	PG 0838+133
085649.3+170115	sdB	13.17	28360 ± 700	5.30 ± 0.15	< −2.6	
090540.9+121228	sdB	14.67	27020 ± 1000	5.38 ± 0.17	−2.70 ^{+0.40} _{−0.60}	PG 0902+124
092308.3+024208 ^a	sdB	14.48	28480 ± 800	5.29 ± 0.16	< −2.6	PG 0920+029
092856.1+061634	sdB	14.29	25020 ± 1100	5.27 ± 0.18	−2.74 ^{+0.40} _{−0.60}	PG 0926+065
093448.2–251248	sdO	13.03	34800 ± 800	5.07 ± 0.24	−2.77 ± 0.62	
095256.6–371940	He-sdO	12.69	43000 ± 1000	5.44 ± 0.30	1.20 ^{+0.50} _{−0.30}	
100752.0–292435	sdB	12.87	41000 ± 950	5.66 ± 0.20	< −2.5	CD–28 7922
104122.8+504420	He-sdO	15.31	51480 ± 1500	5.75 ± 0.15	0.88 ^{+0.50} _{−0.16}	PG 1038+510
104130.4+184210	sdB	13.24	34100 ± 400	5.65 ± 0.12	−1.55 ± 0.13	
104148.9–073031	sdB	12.14	26430 ± 850	5.48 ± 0.14	−2.30 ^{+0.13} _{−0.27}	
110055.9+105542	sdB	14.20	31550 ± 400	5.75 ± 0.13	−1.88 ± 0.16	
110541.4–140423 ^b	sdB+GV	13.0 ^d	(28000)	(5.50)	(−3.0)	EC 11031–1348, FAUST 2814
111422.0–242130	sdB	12.68	21560 ± 1020	5.02 ± 0.20	−2.21 ± 0.40	EC 11119–2405
125941.6+164827 ^a	sdB	14.37	36620 ± 530	5.82 ± 0.13	−1.47 ± 0.13	PG 1257+171
131512.4+024531	sdO	15.10	38980 ± 1150	5.14 ± 0.19	−1.52 ^{+0.42} _{−0.48}	
135629.2–493403	sdB	12.30	32300 ± 530	5.53 ± 0.14	−2.70 ^{+0.42} _{−0.80}	CD–48 8608
135824.6+065137 ^a	sdB	14.50	28120 ± 500	5.45 ± 0.10	−2.96 ± 0.40	PG 1355+071
141055.8+093256 ^a	sdB	14.10	36100 ± 450	5.68 ± 0.11	−1.65 ± 0.13	PG 1408+098
141115.9–305307 ^b	sdB	11.90	26500 ± 2700	5.36 ± 0.26	−1.34 ± 0.24	CD–30 11223, FAUST 3993
143519.8+001350 ^a	sdB	12.50	21650 ± 1050	4.99 ± 0.18	−2.07 ± 0.23	PG 1432+004
145928.5+190350	sdB	14.17	36100 ± 500	5.78 ± 0.12	−1.35 ± 0.11	PG 1457+193
160131.3+044027	He-sdB	14.56	39240 ± 600	5.47 ± 0.16	−0.50 ± 0.11	PG 1559+048
163201.4+075940 ^a	sdO	13.01	34700 ± 900	5.00 ± 0.22	−2.62 ± 0.55	PG 1629+081
173153.7+064706	sdB	13.74	26880 ± 1150	5.29 ± 0.20	−2.80 ^{+0.50} _{−1.10}	
173651.2+280635 ^b	sdB+GV	12.6 ^d	(28000)	(5.50)	(−3.0)	
181032.0+053909	sdB	13.81	31400 ± 450	5.85 ± 0.14	< −2.5	
184559.8–413827	He-sdB	14.63	36400 ± 3200	5.75 ± 0.65	> 1.6	
190302.5–352829	sdB	14.34	32900 ± 900	5.44 ± 0.26	< −2.5	
191109.3–140654 ^b	He-sdO	11.77	50000 ± 2200	5.56 ± 0.32	0.70 ^{+0.50} _{−0.30}	
234947.7+384440 ^{b,c}	sdB	11.71	28400 ± 400	5.40 ± 0.30	−3.20 ± 0.10	FBS 2347+385

^a Strömgren photometry from Wesemael et al. (1992): PG 0314+146 (*y* = 12.525), PG 0838+133 (*y* = 13.653), PG 0920+029 (*y* = 14.395), PG 1257+171 (*y* = 14.276), PG 1355+071 (*y* = 14.307), PG 1408+098 (*y* = 14.115), PG 1432+004 (*y* = 12.759), PG 1629+081 (*y* = 12.779).

^b Also in the bright (*V* < 12) sample.

^c Parameters taken from Kawka et al. (2010a).

^d Based on spectral decomposition (see Section 3.2.1).

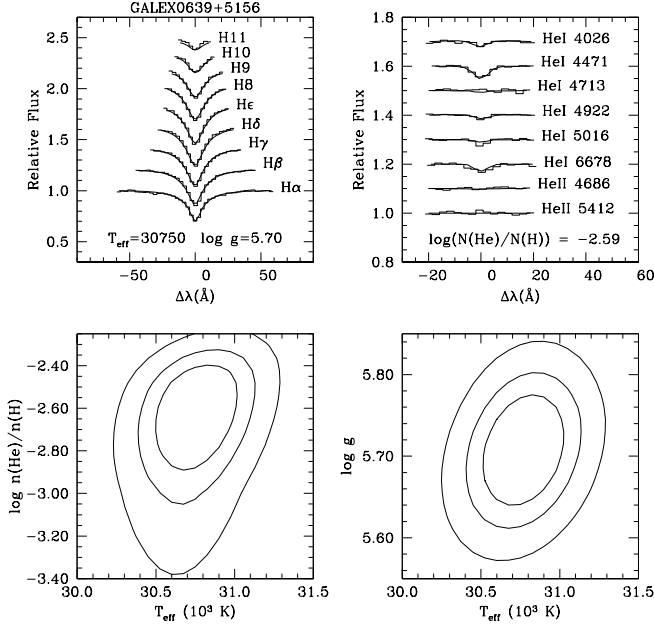


Figure 7. Model atmosphere analysis of the low-dispersion KPNO spectrum of GALEX J0639+5156. The top panels show the line profiles and best-fit models, while the lower panels show the χ^2 contours at 60, 90, and 99%.

liminary spectral decomposition of EC 11031–1348 and GALEX J1736+2806. Based on infrared excess measurements, Ulla & Thejll (1998) found that out of 41 hot subdwarfs, 13 may have G-type companions. The fraction is somewhat lower than found by Thejll, Ulla, & MacDonald (1995) who measured a 50% incidence of binaries in their sample. Figure 9 shows the location of our own sample of hot subdwarf stars in a $V - J$ versus $J - H$ diagram. Most objects cluster close to a sequence defined by single, hot subdwarfs with $V - J, J - H < 0$. A small group of six objects, two of them analysed here (EC 11031–1348, GALEX J1736+2806), are located at $V - J, J - H > 0$ and indicating the presence of a G-type companion in $\approx 1/8$ of our sample.

The subdwarf stars with IR excess are EC 11031–1348 (Kilkenny et al. 1997) which shows composite optical-infrared colours (Reed & Stiening 2004), and the newly spectroscopically identified sdB+GV GALEX J1736+2806. The four other objects with likely F to late G companions are CD-28 1974 (GALEX J0507–2802), CPD-73 420 (GALEX J0657–7324), CD-28 7922 (GALEX J1007–2924) and CD-48 8608 (GALEX J1356–4934). The two subdwarfs with marked composite spectra (EC 11031–1348 and GALEX J1736+2806) are possibly less luminous, hence more easily contaminated in the optical, than the other four objects that show infrared colours typical of G-type stars, but that do not show evidence of a companion in blue spectroscopy.

3.2.2 Overlap with other catalogues of blue stellar objects

Our selection recovered thirteen hot subdwarfs from the Palomar-Green survey (Green, Schmidt, & Liebert 1986): the sdB stars PG 0902+124, PG 0920+029,

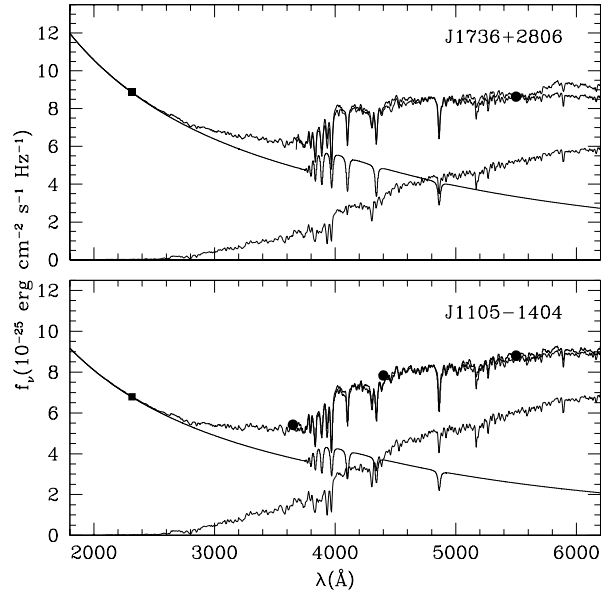


Figure 8. Spectral energy distribution of the sdB+G2V binaries EC 11031–1348 and GALEX J1736+2806 and spectral decompositions. The hot subdwarfs are represented with a model at $T_{\text{eff}} = 28,000$ K and the companion by a G2V template from Pickles (1998). The UBV photometry for EC 11031–1348 is from Kilkenny et al. (1997).

PG 0926+065, PG 1257+171, PG 1335+071, PG 1408+098, PG 1432+004 (Moehler, Heber, & de Boer 1990a; Aznar Cuadrado & Jeffery 2001), PG 1457+193, PG 1559+048, and PG 1629+081, and the sdO stars PG 0314+146 (Aznar Cuadrado & Jeffery 2001), PG 0838+133 (Dreizler et al. 1990; Thejll et al. 1994), and PG 1038+510. A detailed spectroscopic analysis for eight out of ten sdB stars from the PG survey, and two out of three sdO stars from the same survey is presented here for the first time. Wesemael et al. (1992) list Strömgren photometry for eight PG objects from our selection (see Table 2).

Now, we compare the results of our analysis of four PG subdwarfs with the results of previous studies.

PG 0314+146 Using hydrogen models to describe the spectral energy distribution of PG 0314+146 Aznar Cuadrado & Jeffery (2001) derive a relatively low temperature of 20800K. Moreover, Moehler et al. (1990b) observed narrow hydrogen Balmer lines, in contrast to our spectrum which shows broad and shallow HeII lines typical of helium-rich sdO stars. However, Wesemael et al. (1992) noted a discrepancy between their own photometry and that of Moehler et al. (1990b) and concluded that Moehler et al. observed the wrong object. Our GALEX target is located at the coordinates listed by Wesemael et al. The *International Ultraviolet Explorer* (IUE) low-dispersion large-aperture spectrum SWP51740L (Aznar Cuadrado & Jeffery 2001) is peculiar with a broad Ly α line and strong C IV $\lambda 1550$ line, but weaker He II $\lambda 1640$ line. The Ly α line strength is inconsistent with a photospheric origin. Indeed, the equivalent width of $W = 21$ Å implies a neutral hydrogen column density in the line of sight $n_H = 1.9 \times 10^{18} W^2(\text{Å}) = 8 \times$

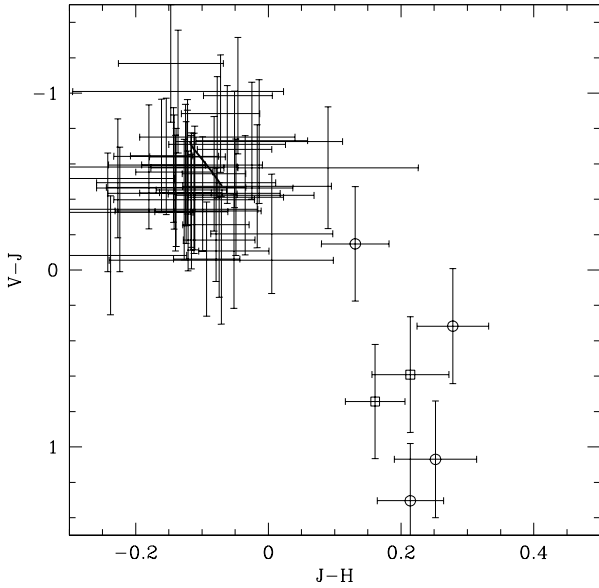


Figure 9. Optical-infrared $V - J$ versus $J - H$ diagram for new hot subdwarfs (Table 2) showing confirmed or likely binaries in the lower-right corner. Confirmed binaries are shown with open squares and suspected binaries with open circles. The companion spectral types range from late F to early G. Most objects cluster near the subdwarf sequence shown with synthetic colours for models at $20000 \leq T_{\text{eff}} \leq 40000$ K and $\log g = 5.7$ (thick line). Note the narrow range of optical-IR colours of hot, single subdwarf stars.

10^{20} cm^{-2} . Following the dust-to-gas relation $n_H/E_{B-V} = 5.8 \times 10^{21} \text{ cm}^{-2}$, the extinction coefficient is predicted to be $E_{B-V} = 0.14$, or $\approx 60\%$ of the total extinction in the line-of-sight toward PG 0314+146 ($E_{B-V} = 0.2267$, Schlegel, Finkbeiner, & Davis 1998). At a Galactic latitude $b = -35.1$ and distance of 300-500 pc (assuming $M_V = 4.2 \pm 0.5$), PG 0314+146 lies 170-290 pc above the plane and the extinction coefficient is expected to be closer to the total extinction in the line-of-sight. In summary, PG 0314+146 is a hot He-sdO with a UV flux distribution showing large interstellar extinction.

PG 0838+133 Our new parameters confirm the analysis of Thejll et al. (1994), $T_{\text{eff}} = 55000$ K, $\log g = 5.8$ and 90% helium ($\log n(\text{He})/n(\text{H}) = 1$), and Dreizler et al. (1990), $T_{\text{eff}} = 44000$, $\log g = 4.8$, $\log n(\text{He})/n(\text{H}) = 1$. We find that the atmosphere is He-rich, as previously determined, and that our new temperature and surface gravity measurements are consistent with the average of the published values.

PG 1432+004 Our new measurements agree with the parameters measured by Moehler, Heber, & de Boer (1990a) that are based on spectroscopy and Strömgren photometry ($T_{\text{eff}} = 22400$ K, $\log g = 5$). However, Aznar Cuadrado & Jeffery (2001) measured $T_{\text{eff}} = 25500 \pm 700$ K at $\log g = 5.5$ based on *IUE* spectra. The *IUE* temperature is significantly higher than the optical measurements possibly because of uncertainties in the interstellar reddening index ($E_{B-V} = 0.07$) determined by Aznar Cuadrado & Jeffery (2001).

PG 1629+081 Allard et al. (1994) and Aznar Cuadrado & Jeffery (2001) noted that PG 1629+081 has a composite optical-UV spectrum. However, their temperature measurements, $T_{\text{eff}} = 32500$ (Allard et al. 1994) and $T_{\text{eff}} = 26400 \pm 1150$ K at $\log g = 5.5$ (Aznar Cuadrado & Jeffery 2001), are lower than expected for a subdwarf showing dominant HeII λ 4686 line. We could not verify the presence of a companion because of the low quality of the 2MASS J photometry.

We recovered two objects from the First Byurakan Survey of blue stellar objects (Mickaelian 2008): FBS 0742+625 classified as B1, and FBS 2347+385 classified as sdB. Our analysis establishes sdB classifications for both objects. We also note from the Hambourg-ESO survey the objects HE 0247-0418 (=PB 9286, Berger & Fringant 1984) and HE 0505-2806 (see Frebel et al. 2006). Berger & Fringant (1984) previously classified PB 9286 as a sdB. Finally, two objects, EC 11031-1348 and EC 11119-2405, are found in the Edinburgh-Cape survey (Kilkenny et al. 1997). Several objects are also included in the Cape Photographic Durchmusterung (CPD) or Cordoba Durchmusterung (CD) catalogues and we listed these names in Table 2 as long as magnitudes and positions ($r < 1'$) are reasonably matched.

Three hot subdwarfs are also listed in the UV catalogues TD-1 and Far-Ultraviolet Space Telescope (FAUST; Bowyer et al. 1995). The source TD1 31206⁵ (Thompson et al. 1978), also known as UVO 0825+15 (Carnochan & Wilson 1983), is listed as an sdO by Berger & Fringant (1980) and in the catalogue of spectroscopically identified subdwarfs of Kilkenny, Heber, & Drilling (1988). The sources FAUST 2814 and FAUST 3993 are also known as EC 11031-1348 (Kilkenny et al. 1997) and CD-30 11223, respectively.

3.2.3 Hot subdwarf evolution

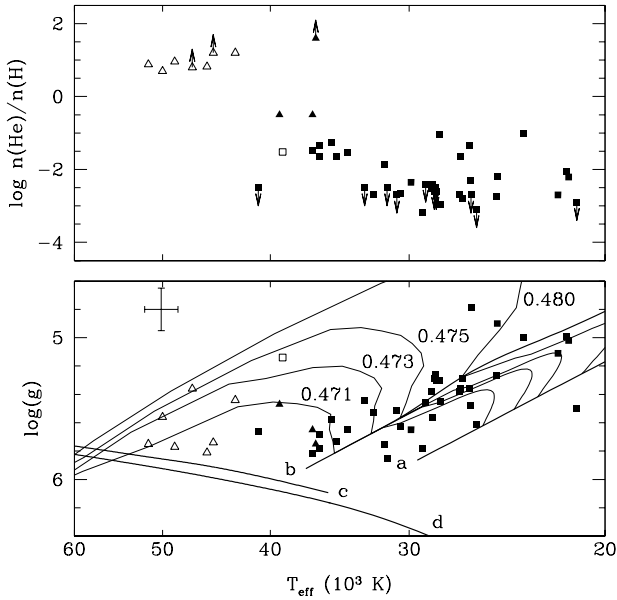
Figure 10 shows the measured parameters in the $\log g$ versus T_{eff} plane and the $\log n(\text{He})/n(\text{H})$ versus T_{eff} planes. The temperature and surface gravity measurements are compared to EHB sequences at 0.471, 0.473, 0.475, and 0.480 M_{\odot} (Dorman, Rood, & O'Connell 1993). The zero-age extreme horizontal-branch and the terminal-age extreme horizontal-branch that marks the exhaustion of helium in the core are labelled ZAEHB and TAEHB, respectively. The location of the helium main sequence (HeMS), covering from 0.33 to 2.0 M_{\odot} is from Divine (1965), Hansen & Spangenberg (1971), and Paczyński (1971a). A class distinction is drawn at $\theta = 0.145$. The 10 hot objects ($\theta < 0.145$) are on average more luminous than the 38 cooler objects ($\theta > 0.145$) and are predominantly He-rich. The average value of $\log g\theta^4$ is 1.9 in the former group while it is 2.5 in the latter. Some He-sdO stars are close to the He-burning main-sequence with masses ranging from 0.75 to 1.0 M_{\odot} as found by Thejll et al. (1994) and are possibly more massive than the average sdB star ($\approx 0.5 M_{\odot}$).

GALEX J0804-1058 is possibly following an evolutionary path similar to the sdB plus WD binary HD 188112 (Heber et al. 2003), and will eventually

⁵ The TD-1 catalogue number 32707 used in Simbad is an error.

Table 3. New white dwarfs selected from colours ($N_{UV} - V < 0.5$) and proper motion ($H > 13$).

GALEX J	V (mag)	$N_{UV} - V$ (mag)	$N_{UV} - J$ (mag)	$J - H$ (mag)	μ (mas yr ⁻¹)	T_{eff} (K)	$\log g$ (cgs)	Notes
041051.6+592501 ^a	14.69	-1.03	-1.18	+0.18	98 ± 7	29990±140	7.80 ± 0.03	2RE J0410+592
045219.3+251935	14.93	-1.07	-1.22	-0.07	110 ± 3	19620±370	8.23 ± 0.06	...
081237.8+173701	13.46	+0.15	-0.15	-0.08	124 ± 3	15260±160	7.82 ± 0.04	...
193156.8+011745 ^b	14.18	-0.63	-1.11	+0.12	61 ± 3	20890±120	7.90 ^{+0.03} _{-0.06}	...
215947.0+293640	15.12	-1.30	-2.01	-0.07	88 ± 2	52850±1850	7.47 ± 0.14	...
232358.7+014025 ^c	14.28	-1.25	-2.01	-0.13	76 ± 4	74300±3600	7.50 ± 0.13	PHL 497

^a Extreme UV source identified by Mason et al. (1995).^b From Vennes, Kawka, & Németh (2010).^c Haro & Luyten (1962); photometry available from Kilkenny (1995).**Figure 10.** Parameters of the *GALEX* sample of sdO (open square), He-sdO (open triangles), sdB (full squares), and He-sdB stars (full triangles). (Top) Helium abundance versus effective temperature measurements showing clear class distinctions. Upper or lower limits are shown with arrows. (Bottom) Surface gravity versus effective temperature measurements compared to evolutionary sequences from Dorman, Rood, & O'Connell (1993) labelled with the corresponding masses. The ZAEHB and TAEHB are marked with the labels “a” and “b”, respectively. The HeMS from (Paczyński 1971a) and Divine (1965) are marked with the labels “c” and “d”, respectively. Typical error bars are shown in the upper left corner.

evolve as an extremely low-mass white dwarf (see Kawka, Vennes, & Vaccaro 2010b). A radial velocity study and search for a potential close companion is under way.

3.3 Properties of the hot white dwarfs

We analysed the white dwarf spectra from H α (or H β) to H $_9$ using the same χ^2 minimization techniques employed in the analysis of the hot subdwarfs. The results of our analysis using the pure-H model grid are summarized in Table 3.

Close inspection of the spectrum of GALEX J1931+0117 suggested that the atmosphere of the star is polluted with heavy elements not normally observed in these objects. Vennes, Kawka, & Németh (2010) presented a detailed analysis of this peculiar white dwarf.

Figure 11 (left) shows hot white dwarfs in a $N_{UV} - J$ versus $J - H$ diagram. Synthetic hot white dwarf colours are listed in Appendix A and the sample of known white dwarfs is described in Appendix B. Composite colours were computed by combining absolute infrared magnitudes for M dwarfs (Kirkpatrick & McCarthy 1994) with white dwarf absolute magnitudes. The white dwarf stars with notable IR excess are located in the lower left corner of the diagram. These objects are: PG0205+134, which was misclassified as a sdO and reclassified as a hot DA (Liebert, Bergeron, & Holberg 2005) with a cool companion (Greenstein 1986; Williams, McGraw, & Grashuis 2001a; Williams et al. 2001b), PG 0824+289 (DA+dC, Heber et al. 1993), GD 123 (DA+dM4.5, Farihi, Becklin, & Zuckerman 2005), PG 1114+187 (DA+dMe, Hillwig, Honeycutt, & Robertson 2000), PG 1123+189 (DA+dM, Green, Ali, & Napiwotzki 2000), HZ 43 which is a hot DA with a crowded dM companion (Greenstein 1986), and the post common-envelope system GD 245 (DA+dMe Schmidt et al. 1995). Most objects fall along single hot white dwarf colours, but the objects with large infrared excess fall close to the WD+dM2 sequence.

Notable IR excess is also apparent in EUVE J1847-223 and EUVE J2124+284 and to a lesser extent in GALEX J0410+5925 and J1931+0117. Vennes, Kawka, & Németh (2010) found a possible link between the infrared excess in GALEX J1931+0117 and the high heavy element abundance in its atmosphere. The infrared excess may be the signature of a debris disc being accreted onto the white dwarf surface. The infrared flux excess in the other three objects remains to be investigated. The case of EUVE 0623-376 illustrates potential problem with the brightest member from the sample. The $N_{UV} - J$ index is affected by inaccurate non-linearity correction of the *GALEX* N_{UV} magnitude measurement. Figure 11 (right) shows the same sample but as a function of white dwarf effective temperatures. Additional objects, that lay hidden in the main white dwarf cooling sequence, show a $N_{UV} - J$ index apparently contaminated by late M dwarf companion (dM4-dM6). The majority of the known DA

white dwarfs closely follow the predicted UV-infrared colour index. About 10% of the white dwarfs have early M dwarf companions (M0-M4) with possibly another 10% having late M dwarf companions (M4-M9). Early-type companions are only detectable in far and extreme ultraviolet selections such as that of TD-1 (Landsman, Simon, & Bergeron 1996) or *EUVE* (Vennes, Christian, & Thorstensen 1998).

4 SUMMARY AND CONCLUSIONS

We presented a new selection of ~ 700 subluminous stars based on the *GALEX* all-sky survey and UV-optical-IR colour indices built using the GSC2.3.2 V_{12} and 2MASS J and H magnitudes. A reduced proper-motion diagram allowed to segregate new white dwarf and subdwarf candidates and spectroscopic follow-up observations uncovered 48 previously unknown or poorly studied hot subdwarf stars, and six new white dwarf stars. Two of the new subdwarfs have been found to be in short-period binaries (Kawka et al. 2010a) while one of the white dwarfs is a rare high-metallicity DAZ white dwarf (Vennes, Kawka, & Németh 2010).

The content of the bright source list ($V \leq 12$) is typical of bright UV surveys such as the TD-1 survey. The list contains primarily blue stars, but also 15 hot subdwarf stars. Nine of the bright subdwarfs were previously unstudied while the sdB star GALEX J0639+5156 and the He-sdO star GALEX J1911-1406 were previously uncatalogued. The bright subdwarf stars are part of a larger list of 52 objects, with 48 of them analysed here for the first time. We found that six of the hot subdwarfs show composite UV-IR colours indicative of F to K type companions, with two of them showing composite sdB plus GV optical spectra. The incidence of binaries in our sample is low ($\sim 12\%$). Thejll, Ulla, & MacDonald (1995) and Ulla & Thejll (1998) found a higher fraction of binaries in their mixed sample of hot subdwarfs ($>20\%$). Williams, McGraw, & Grashuis (2001a); Williams et al. (2001b) also conclude based on IR and optical colour criteria that $\gtrsim 60\%$ of sdO stars have cooler companions, while Jeffery & Pollacco (1998) and Reed & Stiening (2004) found a $\sim 20\%$ incidence of binaries among samples of hot sdB stars. Relatively inaccurate $V-J$ and $J-H$ colour indices are possibly responsible for the lower incidence of binaries in our study.

The stellar parameters T_{eff} and $\log g$ locate the sample of hot subdwarfs along post-EHB evolutionary tracks from the zero-age to the He main-sequence. The abundance of helium in the sample of sdB stars does not correlate with effective temperature $\lesssim 30000$ K, but a shallow trend is observed at $30000 \lesssim T_{\text{eff}} \lesssim 40000$ K (see Edelmann et al. 2003). A clear break in the helium abundance at $T_{\text{eff}} \approx 40000$ K separates He-sdO stars from the other classes. The He-sdB GALEX J1845-4138 is an outstanding case among hot sdB stars. Its helium abundance is comparable to He-sdO stars but with a temperature ~ 4000 K cooler.

Although we were able to report the discovery of several new hot subdwarfs, the bright source list does not contain new white dwarfs. The six new white dwarfs uncovered in this study were selected amongst fainter objects with higher proper-motions ($H > 13$). New white dwarfs may yet be

uncovered amongst unobserved candidates in the range $11 < H < 13$.

Future work on this program will involve a detailed abundance study, in particular for carbon and nitrogen that offer clues to the origin of subdwarfs (e.g., Lanz et al. 2004; Ahmad et al. 2007). The NIII/CIII $\lambda\lambda 4634-4651$ blend is seen in several He-sdO stars. High-dispersion optical and ultraviolet spectroscopy would also enable abundance measurements in sdB stars. For example, Ohl, Chayer, & Moos (2000) measured a metallicity of $0.1\times$ solar in the sdB star PG 0749+658: A more complete abundance pattern would also contribute in improving our $T_{\text{eff}}/\log g$ measurements that are based on H/He model atmospheres (see Edelmann et al. 2003).

Spectroscopic observations and model atmosphere analyses of a second list of objects based on *GALEX* GR6 N_{UV} photometry will be reported in a forthcoming paper.

ACKNOWLEDGMENTS

S.V. and A.K. acknowledge support from the Grant Agency of the Academy of Sciences of the Czech Republic (IAA 300030908, IAA 301630901) and from the Grant Agency of the Czech Republic (GA ČR P209/10/0967). A.K. also acknowledges support from the Centre for Theoretical Astrophysics (LC06014). We thank C. Latham and E. Snape for their assistance with the initial catalogue selection, and R. Østensen for helpful comments on the paper.

REFERENCES

- Allard F., Wesemael F., Fontaine G., Bergeron P., Lamontagne R., 1994, *AJ*, 107, 1565
- Altmann M., Edelmann H., de Boer K. S., 2004, *A&A*, 414, 181
- Ahmad A., Behara N. T., Jeffery C. S., Sahin T., Woolf V. M., 2007, *A&A*, 465, 541
- Aznar Cuadrado R., & Jeffery C. S., 2001, *A&A*, 368, 994
- Aznar Cuadrado R., & Jeffery C. S., 2002, *A&A*, 385, 131
- Barstow M. A., et al., 1994, *MNRAS*, 271, 175
- Benvenuto O. G., Althaus L. G., 1999, *MNRAS*, 303, 30
- Berger J., 1963, *PASP*, 75, 393
- Berger J., Fringant A.-M., 1980, *A&A*, 85, 367
- Berger J., Fringant A.-M., 1984, *A&AS*, 58, 565
- Bergeron P., Saffer R. A., Liebert J., 1992, *ApJ*, 394, 228
- Bergeron P., Wesemael F., Beauchamp A., Wood M. A., Lamontagne R., Fontaine G., Liebert J., 1994, *ApJ*, 432, 305
- Bessell M. S., 1990, *PASP*, 102, 1181
- Billères M., Fontaine G., Brassard P., Liebert J., 2002, *ApJ*, 578, 515
- Bowyer S., Sasseen T.P., Wu X., Lampton M., 1995, *ApJS*, 96, 461
- Caballero J.A., & Solano, E., 2007, *ApJ*, 665, L151
- Caloi V., 1989, *A&A*, 221, 27
- Cardelli J. A., Clayton G. C., Mathis J. S., 1989, *ApJ*, 345, 245
- Carnochan D. J., Wilson R., 1983, *MNRAS*, 202, 317
- Code A. D., Holm A. V., Bottemiller R. L., 1980, *ApJS*, 43, 501

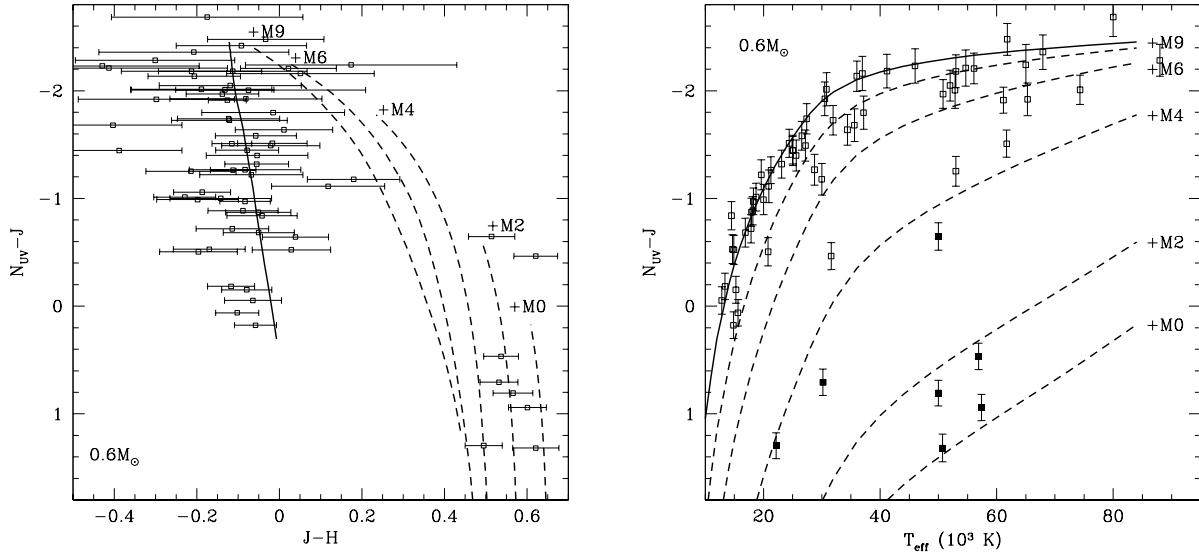


Figure 11. (Left) UV-infrared $N_{UV} - J$ versus $J - H$ diagram for 6 new hot DA white dwarfs (Table 3) and 50 known DA white dwarfs (Table B2) from the present *GALEX* selection. Objects in the lower left corner are known white dwarf plus late-type pairs. The bulk of measurements are close to the hot white dwarf sequence that covers T_{eff} from, top to bottom, 84000 to 12000 K (full line). Composite colours for DA plus dM2, dM4, dM6, and dM9 are shown with dashed lines. (Right) same as left panel but as a function of effective temperatures.

Cohen M., Wheaton W. A., Megeath S. T., 2003, *AJ*, 126, 1090
 Cowley C. R., 1958, *AJ*, 63, 484
 D'Cruz N. L., Dorman B., Rood R. T., O'Connell R. W., 1996, *ApJ*, 466, 359
 Divine N., 1965, *ApJ*, 142, 824
 Dorman B., Rood R. T., O'Connell R. W., 1993, *ApJ*, 419, 596
 Downes R. A., 1986, *ApJS*, 61, 569
 Dreizler S., Heber U., Werner K., Moehler S., & de Boer K. S., 1990, *A&A*, 235, 234
 Dreizler S., Werner K., 1996, *A&A*, 314, 217
 Drilling J. S., Schoenberger D., 1985, *A&A*, 146, L23
 Dupuis J., Vennes S., Chayer P., Hurwitz M., Bowyer S., 1998, *ApJ*, 500, L45
 Edelmann H., Heber U., Altmann M., Karl C., Lisker T., 2005, *A&A*, 442, 1023
 Edelmann H., Heber U., Hagen H.-J., Lemke M., Dreizler S., Napiwotzki R., Engels D., 2003, *A&A*, 400, 939
 Eisenstein D. J., et al., 2006, *ApJS*, 167, 40
 Farihi J., Becklin E. E., Zuckerman B., 2005, *ApJS*, 161, 394
 Feige J., 1958, *ApJ*, 128, 267
 Feast M.W., Thackeray A.D., & Wesselink A.J., 1960, *MNRAS*, 121, 337
 Frebel A., et al., 2006, *ApJ*, 652, 1585
 Giclas H. L., Burnham R., Jr., Thomas N. G., 1965, *LowOB*, 6, 155
 Giclas H. L., Burnham R., Jr., Thomas N. G., 1980, *LowOB*, 8, 157
 Gould N. L., Herbig G. H., Morgan W. W., 1957, *PASP*, 69, 242
 Green R. F., 1980, *ApJ*, 238, 685
 Green P. J., Ali B., Napiwotzki R., 2000, *ApJ*, 540, 992

Green R. F., Schmidt M., Liebert J., 1986, *ApJS*, 61, 305
 Greenstein J. L., 1966, *ApJ*, 144, 496
 Greenstein J. L., 1986, *AJ*, 92, 867
 Greenstein J.L. & Sargent A.I., 1974, *ApJS*, 28, 157
 Han Z., Podsiadlowski Ph., Maxted P.F.L., Marsh T.R., Ivanova N., 2002, *MNRAS*, 336, 449
 Han Z., Podsiadlowski Ph., Maxted P.F.L., Marsh T.R., 2003, *MNRAS*, 341, 669
 Hansen C. J., & Spangenberg W. H., 1971, *ApJ*, 168, 71
 Haro G., Luyten W. J., 1962, *BOTT*, 3, 37
 Heber U., 1986, *A&A*, 155, 33
 Heber U., 2009, *ARAA*, 47, 211
 Heber U., Bade N., Jordan S., Voges W., 1993, *A&A*, 267, L31
 Heber U., Dreizler S., Hagen H.-J., 1996, *A&A*, 311, L17
 Heber U., Edelmann H., Lisker T., Napiwotzki R., 2003, *A&A*, 411, L477
 Hillwig T. C., Honeycutt R. K., Robertson J. W., 2000, *AJ*, 120, 1113
 Holberg J. B., et al., 1993, *ApJ*, 416, 806
 Holm A. V., 1976, *ApJ*, 210, L87
 Hubeny I., Lanz T., 1995, *ApJ*, 439, 875
 Humason M. L., Zwicky F., 1947, *ApJ*, 105, 85
 Iriarte B., Chavira E., 1957, *BOTT*, 2, 3
 Jaschek M., Jaschek C., 1963, *PASP*, 75, 365
 Jeffery C. S., Pollacco D. L., 1998, *MNRAS*, 298, 179
 Jordan S., Heber U., Engels D., Koester D., 1993, *A&A*, 273, L27
 Jordan S., et al., 1998, *A&A*, 330, 277
 Kalirai J. S., Hansen B. M. S., Kelson D. D., Reitzel D. B., Rich R. M., Richer H. B., 2008, *ApJ*, 676, 594
 Kawka A., Vennes S., 2006, *ApJ*, 643, 402
 Kawka A., Vennes S., Nemeth P., Kraus M., Kubat J., 2010a, *MNRAS*, in press (DOI: 10.1111/j.1365-

- 2966.2010.17165.x)
- Kawka A., Vennes S., Vaccaro T. R., 2010b, *A&A*, 516, L7
- Kawka A., Vennes S., Schmidt G. D., Wickramasinghe D. T., Koch R., 2007, *ApJ*, 654, 499
- Kilkenny D., 1995, *MNRAS*, 277, 920
- Kilkenny D., Heber U., Drilling J. S., 1988, *SAAOC*, 12, 1
- Kilkenny D., O'Donoghue D., Koen C., Stobie R. S., & Chen A., 1997, *MNRAS*, 287, 867
- Kirkpatrick J. D., McCarthy D. W., Jr., 1994, *AJ*, 107, 333
- Koester D., Liebert J., Saffer R. A., 1994, *ApJ*, 422, 783
- Lamontagne R., Demers S., Wesemael F., Fontaine G., Irwin M. J., 2000, *AJ*, 119, 241
- Landsman W., Simon T., Bergeron P., 1996, *PASP*, 108, 250
- Lanz T., Brown T. M., Sweigart A. V., Hubeny I., Landsman W. B., 2004, *ApJ*, 602, 342
- Lanz T., Hubeny I., 1995, *ApJ*, 439, 905
- Lasker B. M., et al., 2008, *AJ*, 136, 735
- Lemke M., 1997, *A&AS*, 122, 285
- Lépine S., Shara M. M., 2005, *AJ*, 129, 1483
- Liebert J., Bergeron P., Holberg J. B., 2005, *ApJS*, 156, 47
- Luyten W.J., 1963, *Bruce proper motion survey: The general catalogue*, Vol. I-II (Minneapolis: Univ. Minnesota)
- Luyten W.J., 1979, *New Luyten Catalogue of Stars with Proper Motions Larger than Two Tenths of an Arcsecond*, Vol. I-II (Minneapolis: Univ. Minnesota)
- Luyten W.J., 1980, *New Luyten Catalogue of Stars with Proper Motions Larger than Two Tenths of an Arcsecond*, Vol. III-IV (Minneapolis: Univ. Minnesota)
- Mason K. O., et al., 1995, *MNRAS*, 274, 1194
- Maxted P. f. L., Heber U., Marsh T. R., & North R. C., 2001, *MNRAS*, 326, 1391
- Mengel J.G., Norris J., Gross P.G., 1976, *ApJ*, 204, 488
- Mereghetti S., Tiengo A., Esposito P., La Palombara N., Israel G. L., Stella L., 2009, *Sci*, 325, 1222
- Mickaelian A.M., 2008, *AJ*, 136, 946
- Mitchell K. J., 1998, *ApJ*, 494, 256
- Moehler S., Heber U., de Boer K. S., 1990a, *A&A*, 239, 265
- Moehler S., Richtler T., de Boer K. S., Dettmar R. J., Heber U., 1990b, *A&AS*, 86, 53
- Morales-Rueda L., Maxted P.F.L., Marsh T.R., North R.C., Heber U., 2003, *MNRAS*, 338, 752
- Morrissey P., et al., 2007, *ApJS*, 173, 682
- Newcomer R.E., Murthy J., Henry R.C., Price S.D., Paxton L., 2004, *Air Force Research Laboratory Technical Report AFRL-VS-TR-2004-1056*
- Ochsenbein F., Bauer P., Marcout J., 2000, *A&AS*, 143, 23
- O'Donoghue D., Lynas-Gray A. E., Kilkenny D., Stobie R. S., Koen C., 1997, *MNRAS*, 285, 657
- Ohl R. G., Chayer P., Moos H. W., 2000, *ApJ*, 538, L95
- Østensen R. H., et al., 2010, *A&A*, 513, A6
- Paczýński B., 1971a, *Acta Astronomica*, 21, 1
- Paczýński B., 1971b, *Acta Astronomica*, 21, 417
- Pickles A.J., 1998, *PASP*, 110, 863
- Ramspeck M., Heber U., Edelmann H., 2001, *A&A*, 379, 235
- Reed M. D., & Stiening R., 2004, *PASP*, 116, 506
- Russell J. L., Lasker B. M., McLean B. J., Sturch C. R., Jenkner H., 1990, *AJ*, 99, 2059
- Saffer R. A., Bergeron P., Koester D., & Liebert J., 1994, *ApJ*, 432, 351
- Salim S., Gould A., 2003, *ApJ*, 582, 1011
- Schlegel D. J., Finkbeiner D. P., Davis M., 1998, *ApJ*, 500, 525
- Schmidt G. D., Smith P. S., Harvey D. A., Grauer A. D., 1995, *AJ*, 110, 398
- Schoenberger D., 1983, *ApJ*, 272, 708
- Sion E. M., Fritz M. L., McMullin J. P., Lallo M. D., 1988, *AJ*, 96, 251
- Skrutskie M. F., et al., 2006, *AJ*, 131, 1163
- Slettebak A., Bahner K., Stock J., 1961, *ApJ*, 134, 195
- Smith Neubig M.M., & Bruhweiler F.C., 1999, *AJ*, 117, 2856
- Stroeer A., Heber U., Lisker T., Napiwotzki R., Dreizler S., Christlieb N., Reimers D., 2007, *A&A*, 462, 269
- Soubiran C., et al., 2008, *sf2a.conf*, 35
- Stark M. A., Wade R. A., 2003, *AJ*, 126, 1455
- Sweigart A. V., 1997a, *ApJ*, 474, L23
- Sweigart A. V., 1997b, *The Third Conference on Faint Blue Stars (Schenectady: L. Davis Press)*, 3
- Sweigart A. V., Mengel J. G., Demarque P., 1974, *A&A*, 30, 13
- Thejll P., Bauer F., Saffer R., Liebert J., Kunze D., & Shipman H. L., 1994, *ApJ*, 433, 819
- Thejll P., Flynn C., Williamson R., Saffer R., 1997, *A&A*, 317, 689
- Thejll P., Ulla A., MacDonald J., 1995, *A&A*, 303, 773
- Thejll P., Vennes S., Shipman H. L., 1991, *ApJ*, 370, 355
- Thompson G. I., Nandy K., Jamar C., Monfils A., Houzi- aux L., Carnochan D. J., Wilson R., 1978, *Catalogue of Stellar Ultraviolet Fluxes (TD-1)*. The Science Research Council, UK
- Tremblay P.-E., Bergeron P., 2009, *ApJ*, 696, 1755
- Ulla A., & Thejll P., 1998, *A&AS*, 132, 1
- Vassiliadis E., Wood P. R., 1993, *ApJ*, 413, 641
- Vennes S., 1999, *ApJ*, 525, 995
- Vennes S., Christian D. J., Thorstensen J. R., 1998, *ApJ*, 502, 763
- Vennes S., Kawka A., Németh P., 2010, *MNRAS*, 404, L40
- Vennes S., Kawka A., Smith J.A., 2007, *ApJ*, 668, L59
- Vennes S., Korpela E., Bowyer S., 1997, *AJ*, 114, 1567
- Vennes S., Smith R.J., Boyle B.J., Croom S. M., Kawka A., Shanks T., Miller L., Loaring N., 2002, *MNRAS*, 335, 673
- Vennes S., Thejll P. A., Galvan R. G., Dupuis J., 1997, *ApJ*, 480, 714
- Wagner R. M., Sion E. M., Liebert J., Starrfield S. G., 1988, *ApJ*, 328, 213
- Wegner G., Swanson S. R., 1990, *AJ*, 99, 330
- Weidemann V., 2000, *A&A*, 363, 647
- Werner K., Rauch T., Kruk J. W., 2008, *A&A*, 492, L43
- Wesemael F., Fontaine G., Bergeron P., Lamontagne R., & Green R. F., 1992, *AJ*, 104, 203
- Wesselius P. R., van Duinen R. J., de Jonge A. R. W., Aalders J. W. G., Luinge W., Wildeman K. J., 1982, *A&AS*, 49, 427
- Wesselius P. R., Koester D., 1978, *A&A*, 70, 745
- Williams T., McGraw J. T., Grashuis R., 2001a, *PASP*, 113, 490
- Williams T., McGraw J. T., Mason P. A., Grashuis R., 2001b, *PASP*, 113, 944
- Wood M.A., 1995, *LNP*, 443, 41
- Zacharias N., Monet D. G., Levine S. E., Urban S. E., Gaume R., Wycoff G. L., 2004, *AAS*, 36, 1418

Zhang X., Chen X., Han Z., 2009, A&A, 504, L13

APPENDIX A: ULTRAVIOLET, VISUAL, AND INFRARED MAGNITUDES FOR WHITE DWARFS

Table A1 lists absolute *GALEX* N_{UV} and F_{UV} magnitudes, Johnson V magnitude, and the 2MASS J and H magnitudes for white dwarfs of 0.4, 0.5, 0.6, 0.8, 1.0 and 1.2 M_{\odot} . The absolute calibration employs the mass-radius relations of Wood (1995) and Benvenuto & Althaus (1999). We calculated the absolute ultraviolet magnitudes N_{UV} and F_{UV} in the AB system and using the post-launch response curves⁶. Next, we calculated the Johnson V and 2MASS magnitudes using the response curves and zero-points of Bessell (1990) and Cohen, Wheaton, & Megeath (2003), respectively. Figure A1 shows colour indices for all masses and between 12000 and 84000 K. The $F_{UV} - N_{UV}$ index is sensitive to surface gravity, hence mass, at lower temperatures. With increasing surface gravity, the extended Ly α line wing and the Lyman satellites act to depress the continuum in the F_{UV} band. The synthetic colours are computed with pure hydrogen models and do not take into account the effect of metallicity. The colours should also be corrected for the effect of interstellar reddening as needed.

APPENDIX B: A SAMPLE OF BRIGHT WHITE DWARFS IN THE GALEX ALL-SKY SURVEY

Table B1 lists colours and effective temperatures of known non-DA white dwarfs (DAB, DAO, DB, DO) recovered in our *GALEX*-GSC selection. The reference for the tabulated effective temperature and the usual name are also listed. Table B2 provides the same information as Table B1 but for the DA white dwarfs.

⁶ Available at <http://galexgi.gsfc.nasa.gov/docs/galex/Documents/PostLaunchResponseCurveData.html>.

Table A1. Absolute ultraviolet, optical, and infrared magnitudes as a function of white dwarf effective temperatures and masses.

T_{eff} (10^3 K)	F_{UV} (mag)	N_{UV} (mag)	V (mag)	J (mag)	H (mag)	T_{eff} (10^3 K)	F_{UV} (mag)	N_{UV} (mag)	V (mag)	J (mag)	H (mag)
0.4 M_{\odot}						0.5 M_{\odot}					
10.0	15.103	12.631	11.622	11.574	11.530	10.0	15.538	12.912	11.921	11.862	11.813
11.0	13.381	12.067	11.289	11.405	11.401	11.0	13.819	12.353	11.591	11.699	11.688
12.0	12.127	11.644	11.079	11.297	11.310	12.0	12.566	11.910	11.368	11.588	11.599
13.0	11.372	11.273	10.908	11.198	11.221	13.0	11.710	11.565	11.217	11.506	11.526
14.0	10.902	10.928	10.739	11.082	11.115	14.0	11.210	11.226	11.055	11.401	11.431
15.0	10.526	10.629	10.595	10.978	11.018	15.0	10.827	10.929	10.912	11.300	11.338
16.0	10.192	10.356	10.461	10.877	10.924	16.0	10.501	10.668	10.789	11.210	11.255
18.0	9.607	9.867	10.210	10.682	10.740	18.0	9.937	10.203	10.560	11.038	11.095
20.0	9.104	9.443	9.982	10.503	10.570	20.0	9.455	9.801	10.353	10.880	10.946
22.0	8.658	9.065	9.770	10.335	10.410	22.0	9.029	9.443	10.161	10.730	10.804
24.0	8.246	8.711	9.561	10.165	10.248	24.0	8.643	9.114	9.976	10.584	10.666
26.0	7.869	8.378	9.357	9.998	10.088	26.0	8.292	8.806	9.795	10.441	10.530
28.0	7.522	8.058	9.151	9.825	9.923	28.0	7.971	8.511	9.612	10.291	10.388
30.0	7.210	7.758	8.944	9.645	9.749	30.0	7.687	8.237	9.430	10.134	10.238
32.0	6.940	7.493	8.751	9.470	9.579	32.0	7.442	7.997	9.260	9.982	10.089
36.0	6.505	7.071	8.424	9.165	9.277	36.0	7.054	7.622	8.978	9.721	9.833
40.0	6.166	6.748	8.162	8.916	9.031	40.0	6.757	7.341	8.757	9.513	9.627
44.0	5.879	6.476	7.934	8.697	8.813	44.0	6.502	7.101	8.561	9.325	9.441
48.0	5.626	6.236	7.729	8.498	8.615	48.0	6.272	6.885	8.378	9.149	9.266
52.0	5.388	6.011	7.531	8.307	8.424	52.0	6.051	6.676	8.197	8.974	9.091
56.0	5.159	5.793	7.337	8.117	8.236	56.0	5.841	6.476	8.021	8.802	8.920
60.0	4.933	5.576	7.141	7.925	8.044	60.0	5.629	6.274	7.838	8.624	8.743
64.0	4.700	5.352	6.934	7.723	7.842	64.0	5.426	6.079	7.661	8.451	8.570
68.0	4.455	5.116	6.715	7.507	7.627	68.0	5.220	5.882	7.480	8.272	8.392
72.0	4.193	4.861	6.475	7.270	7.391	72.0	5.018	5.687	7.299	8.095	8.216
76.0	3.912	4.587	6.215	7.013	7.135	76.0	4.806	5.482	7.107	7.905	8.026
80.0	3.593	4.274	5.914	6.715	6.838	80.0	4.594	5.276	6.912	7.714	7.835
84.0	3.175	3.862	5.514	6.318	6.441	84.0	4.374	5.062	6.709	7.513	7.636
0.6 M_{\odot}						0.8 M_{\odot}					
10.0	15.898	13.158	12.182	12.115	12.062	10.0	16.545	13.633	12.681	12.600	12.540
11.0	14.195	12.603	11.854	11.953	11.938	11.0	14.902	13.077	12.349	12.435	12.411
12.0	12.952	12.142	11.617	11.836	11.843	12.0	13.606	12.606	12.100	12.309	12.309
13.0	12.016	11.813	11.477	11.763	11.780	13.0	12.634	12.259	11.946	12.232	12.244
14.0	11.478	11.482	11.327	11.673	11.700	14.0	11.990	11.950	11.818	12.161	12.182
15.0	11.088	11.188	11.186	11.577	11.613	15.0	11.566	11.655	11.679	12.074	12.105
16.0	10.758	10.926	11.061	11.487	11.530	16.0	11.231	11.398	11.560	11.992	12.031
18.0	10.202	10.473	10.843	11.325	11.380	18.0	10.676	10.953	11.346	11.836	11.887
20.0	9.729	10.081	10.645	11.176	11.240	20.0	10.211	10.572	11.157	11.695	11.757
22.0	9.311	9.730	10.458	11.032	11.105	22.0	9.810	10.239	10.987	11.567	11.638
24.0	8.939	9.415	10.287	10.899	10.980	24.0	9.448	9.933	10.822	11.442	11.521
26.0	8.601	9.119	10.117	10.766	10.854	26.0	9.123	9.648	10.662	11.317	11.404
28.0	8.294	8.837	9.945	10.627	10.723	28.0	8.832	9.380	10.501	11.188	11.283
30.0	8.025	8.577	9.776	10.482	10.585	30.0	8.577	9.132	10.341	11.053	11.153
32.0	7.797	8.354	9.620	10.344	10.451	32.0	8.364	8.923	10.197	10.925	11.029
36.0	7.438	8.007	9.366	10.110	10.221	36.0	8.038	8.609	9.973	10.720	10.829
40.0	7.171	7.756	9.174	9.931	10.044	40.0	7.800	8.386	9.808	10.567	10.679
44.0	6.952	7.551	9.013	9.778	9.893	44.0	7.606	8.208	9.672	10.439	10.553
48.0	6.758	7.372	8.867	9.639	9.755	48.0	7.443	8.058	9.555	10.329	10.445
52.0	6.583	7.209	8.731	9.509	9.626	52.0	7.299	7.925	9.450	10.229	10.345
56.0	6.419	7.055	8.601	9.383	9.501	56.0	7.169	7.807	9.354	10.138	10.255
60.0	6.261	6.907	8.472	9.259	9.377	60.0	7.049	7.696	9.263	10.051	10.169
64.0	6.105	6.760	8.343	9.133	9.252	64.0	6.936	7.592	9.176	9.968	10.087
68.0	5.951	6.614	8.212	9.005	9.125	68.0	6.830	7.493	9.093	9.888	10.007
72.0	5.796	6.466	8.078	8.874	8.995	72.0	6.726	7.398	9.011	9.809	9.929
76.0	5.636	6.313	7.938	8.737	8.858	76.0	6.628	7.306	8.931	9.732	9.853
80.0	5.470	6.153	7.789	8.592	8.713	80.0	6.533	7.217	8.854	9.657	9.778
84.0	5.300	5.989	7.637	8.441	8.563	84.0	6.437	7.127	8.774	9.580	9.702

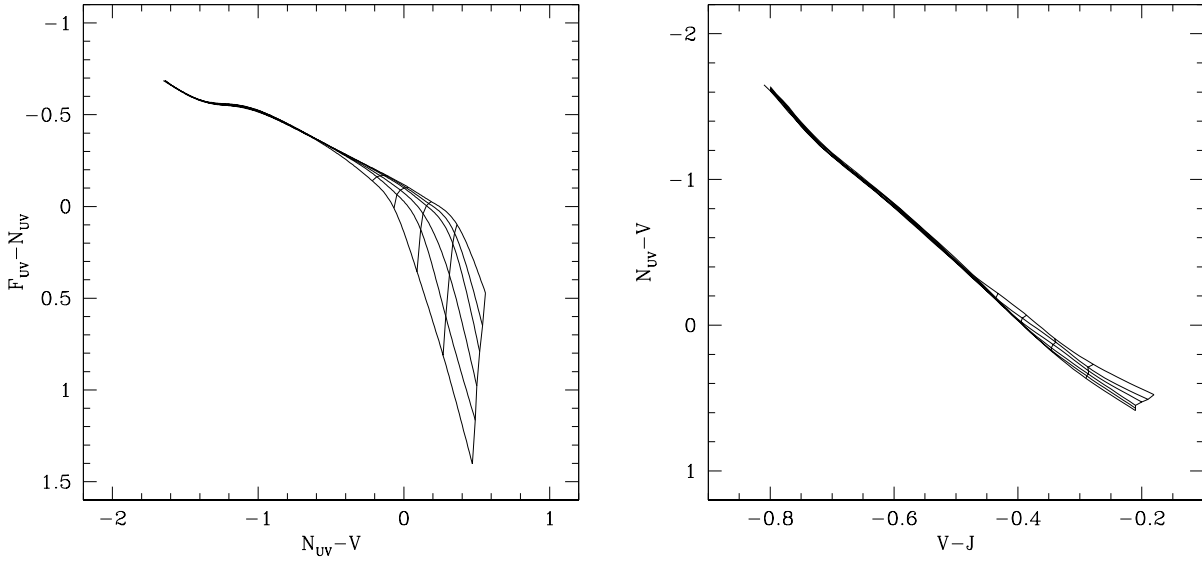


Figure A1. (Left) $F_{UV} - N_{UV}$ versus $N_{UV} - V$ colour indices for white dwarfs at, from top to bottom, 0.4, 0.5, 0.6, 0.8, 1.0, and 1.2 M_{\odot} and $12000 \leq T_{\text{eff}} \leq 84000$ K, and (right) $N_{UV} - V$ versus $V - J$ for the same masses and temperatures.

Table A1 – *continued*

T_{eff} (10^3 K)	F_{UV} (mag)	N_{UV} (mag)	V (mag)	J (mag)	H (mag)	T_{eff} (10^3 K)	F_{UV} (mag)	N_{UV} (mag)	V (mag)	J (mag)	H (mag)
1.0 M_{\odot}						1.2 M_{\odot}					
10.0	17.215	14.156	13.228	13.134	13.069	10.0	18.175	14.949	14.055	13.944	13.872
11.0	15.660	13.603	12.896	12.968	12.937	11.0	16.757	14.403	13.726	13.780	13.741
12.0	14.297	13.129	12.638	12.837	12.829	12.0	15.337	13.931	13.460	13.643	13.627
13.0	13.346	12.745	12.457	12.744	12.751	13.0	14.341	13.530	13.261	13.539	13.538
14.0	12.587	12.460	12.344	12.683	12.698	14.0	13.568	13.213	13.123	13.464	13.473
15.0	12.106	12.171	12.219	12.612	12.636	15.0	12.967	12.958	13.026	13.412	13.429
16.0	11.749	11.911	12.097	12.533	12.567	16.0	12.560	12.700	12.917	13.349	13.375
18.0	11.185	11.468	11.885	12.382	12.430	18.0	11.970	12.255	12.705	13.210	13.252
20.0	10.724	11.094	11.701	12.246	12.305	20.0	11.504	11.883	12.520	13.075	13.129
22.0	10.326	10.765	11.532	12.120	12.187	22.0	11.111	11.560	12.356	12.953	13.017
24.0	9.972	10.465	11.372	11.999	12.075	24.0	10.766	11.269	12.202	12.837	12.910
26.0	9.658	10.189	11.219	11.881	11.965	26.0	10.460	10.998	12.051	12.721	12.803
28.0	9.377	9.928	11.063	11.756	11.848	28.0	10.193	10.748	11.902	12.601	12.691
30.0	9.135	9.693	10.911	11.627	11.726	30.0	9.964	10.524	11.758	12.478	12.574
32.0	8.932	9.493	10.775	11.506	11.609	32.0	9.774	10.338	11.630	12.364	12.465
36.0	8.624	9.197	10.565	11.315	11.423	36.0	9.488	10.063	11.438	12.190	12.296
40.0	8.397	8.986	10.410	11.172	11.283	40.0	9.276	9.866	11.296	12.059	12.169
44.0	8.220	8.822	10.289	11.058	11.172	44.0	9.110	9.715	11.185	11.957	12.069
48.0	8.068	8.684	10.183	10.959	11.074	48.0	8.971	9.588	11.091	11.869	11.983
52.0	7.934	8.562	10.088	10.870	10.985	52.0	8.849	9.478	11.007	11.791	11.907
56.0	7.819	8.457	10.006	10.792	10.909	56.0	8.741	9.380	10.932	11.720	11.837
60.0	7.710	8.358	9.926	10.716	10.834	60.0	8.642	9.291	10.862	11.654	11.772
64.0	7.611	8.267	9.853	10.646	10.765	64.0	8.555	9.212	10.800	11.596	11.714
68.0	7.519	8.183	9.784	10.581	10.700	68.0	8.475	9.140	10.743	11.542	11.662
72.0	7.432	8.104	9.718	10.518	10.637	72.0	8.402	9.074	10.690	11.492	11.613
76.0	7.349	8.028	9.654	10.457	10.577	76.0	8.333	9.012	10.640	11.445	11.566
80.0	7.270	7.955	9.592	10.398	10.519	80.0	8.268	8.953	10.593	11.401	11.522
84.0	7.193	7.883	9.531	10.339	10.460	84.0	8.207	8.897	10.547	11.357	11.479

Table B1. Colours and temperatures of known non-DA white dwarfs in the *GALEX* selection.

R.A.(J2000)	Dec.(J2000)	$N_{\text{UV}} - J$ (mag)	$J - H$ (mag)	T_{eff} (10^3 K)	Name	Sp. Type	Reference ^a
00 08 18.2	+51 23 15.1	−1.06	−0.19	200.0	KPD 0005+5106	DO	(1)
00 41 35.4	+20 09 17.4	−2.42	−0.09	115.0	PG 0038+199	DO	(2)
01 13 46.7	+00 28 30.9	−2.24	0.17	65.0	HS 0111+0012	DO	(2)
02 12 04.8	+08 46 49.8	−2.13	−0.21	36.0	HS 0209+0832	DAB	(3)
05 08 31.0	+01 16 41.3	−2.68	−0.18	80:	HS 0505+0112	DAO	(4)
12 13 56.3	+32 56 33.1	−2.18	−0.21	53.0	HZ 21	DO	(2)
13 04 32.0	+59 27 33.8	−1.27	−0.08	28.8	GD 323	DAB	(5)
16 47 18.5	+32 28 31.8	−1.45	−0.08	25.0	GD 358	DB	(6)
23 45 02.9	+80 56 59.0	−1.92	−0.30	65.3	GD 561	DAO	(7)

^a REFERENCES: (1) Werner, Rauch, & Kruk (2008); (2) Dreizler & Werner (1996); (3) Jordan et al. (1993); (4) Heber, Dreizler, & Hagen (1996); (5) Koester, Liebert, & Saffer (1994); (6) Thejll, Vennes, & Shipman (1991); (7) Bergeron et al. (1994).

Table B2. Colours and temperatures of known DA white dwarfs in the *GALEX* selection.

R.A.(J2000)	Dec.(J2000)	$N_{UV} - J$ (mag)	$J - H$ (mag)	T_{eff} (10^3 K)	Name	Sp. Type	Reference ^a
00 07 32.1	+33 17 27.2	-1.97	-0.14	50.8	GD 2	DA	(1)
00 39 52.2	+31 32 26.4	-2.05	-0.12	52.0	GD 8	DA	(2)
00 53 40.5	+36 01 16.6	-1.74	-0.12	27.4	EUVE 0053+360	DA	(1)
01 04 41.2	+09 49 42.7	-1.40	-0.05	25.6	PG 0102+096	DA	(2)
01 41 28.7	+83 34 56.9	-1.01	-0.23	18.7	GD 419	DA	(3)
02 08 03.4	+13 36 24.6	0.94	0.60	57.4	PG 0205+134	DA	(4)
02 18 48.0	+14 36 06.2	-1.49	-0.02	27.2	PG 0216+144	DA	(1)
03 04 37.2	+02 56 58.0	-1.68	-0.40	35.6	GD 41	DA	(1)
03 11 49.1	+19 00 56.1	-0.72	-0.11	17.9	PG 0308+188	DA	(4)
04 12 43.5	+11 51 47.7	-0.51	-0.20	20.8	HZ 2	DA	(3)
04 28 39.4	+16 58 12.4	-1.51	-0.02	24.4	EGGR 37	DA	(2)
05 05 30.7	+52 49 50.1	-1.91	-0.13	61.2	G191 B2B	DA	(1)
05 10 14.0	+04 38 37.3	-0.99	-0.20	20.0	HS 0507+0434A	DA	(5)
06 23 12.8	-37 41 25.0	-1.51	-0.11	61.7	EUVE 0623-376	DA	(1)
08 27 05.1	+28 44 02.2	1.32	0.62	50.7	PG 0824+289	DA	(4)
08 42 53.0	+23 00 25.9	-1.45	-0.39	25.0	PG 0839+232	DA	(4)
09 42 50.7	+26 00 58.6	-2.36	-0.21	67.9	PG 0824+289	DA	(4)
09 46 39.1	+43 54 54.9	-0.05	-0.06	12.8	PG 0943+441	DA	(4)
09 48 46.7	+24 21 25.4	-0.84	-0.04	14.5	PG 0945+246	DA	(4)
10 36 25.2	+46 08 27.9	0.71	0.53	30.2	GD 123	DA	(1)
10 44 45.7	+57 44 35.7	-2.01	-0.19	30.8	PG 1041+580	DA	(1)
10 54 43.4	+27 06 58.4	-1.32	-0.05	23.1	PG 1051+274	DA	(4)
11 00 34.4	+71 38 03.5	-2.18	-0.11	41.2	PG 1057+719	DA	(1)
11 07 42.6	+59 58 28.3	-0.87	-0.05	17.9	EGGR 75	DA	(3)
11 17 03.7	+18 25 58.1	-0.65	0.51	50:	PG 1114+187	DA+dMe	(6)
11 26 19.1	+18 39 14.8	0.47	0.54	56.9	PG 1123+189	DA	(1)
11 32 27.4	+15 17 29.4	-0.68	-0.05	16.9	PG 1129+156	DA	(4)
11 37 05.2	+29 47 57.6	-1.26	-0.11	21.3	PG 1134+301	DA	(4)
11 43 59.5	+07 29 04.4	-2.48	-0.03	61.8	PG 1141+078	DA	(4)
11 45 56.7	+31 49 29.5	-0.52	0.03	14.9	PG 1143+321	DA	(4)
11 48 03.2	+18 30 46.3	-1.58	-0.06	26.6	PG 1145+188	DA	(1)
12 12 33.9	+13 46 26.6	-1.73	-0.12	31.9	PG 1210+141	DA	(4)
12 36 44.8	+47 55 20.6	-2.21	0.02	56.1	PG 1234+481	DA	(1)
13 16 21.8	+29 05 57.8	0.81	0.57	50.0	HZ 43	DA	(7)
13 46 01.9	+57 00 33.7	-0.18	-0.12	13.4	PG 1344+573	DA	(4)
14 10 27.1	+32 08 33.8	-0.89	-0.09	18.1	PG 1408+324	DA	(4)
16 02 42.1	+57 58 16.0	-0.53	-0.17	14.7	PG 1601+581	DA	(4)
16 05 21.1	+43 04 36.0	-2.16	0.05	37.0	PG 1603+432	DA	(4)
16 38 26.4	+35 00 12.3	-1.80	-0.01	37.2	EUVE 1638+349	DA	(1)
16 59 48.3	+44 01 04.1	-1.92	-0.08	30.5	PG 1658+441	DA	(4)
17 13 05.8	+69 31 23.2	0.06	-0.10	15.6	EGGR 370	DA	(3)
17 38 02.8	+66 53 46.7	-2.28	-0.30	88.0	RE 1738+665	DA	(8)
18 00 09.7	+68 35 52.7	-2.23	-0.43	46.0	KUV 18004+6836	DA	(1)
18 47 56.6	-22 19 40.6	-0.47	0.62	31.6	EUVE 1847-223	DA	(1)
19 43 43.8	+50 04 38.9	-1.64	0.01	34.4	EUVE 1943+500	DA	(1)
20 10 56.7	-30 13 09.9	0.18	-0.06	14.8	LTT 7987	DA	(9)
21 16 53.1	+73 50 41.0	-2.21	-0.41	54.7	KUV 21168+7338	DA	(1)
21 24 58.1	+28 26 03.2	-1.25	-0.21	53.0	EUVE 2124+284	DA	(10)
21 52 25.2	+02 23 18.6	-0.97	-0.08	18.2	EGGR 150	DA	(3)
22 58 48.2	+25 15 43.4	1.29	0.49	22.2	GD 245	DA+dMe	(11)

^a REFERENCES: (1) Vennes et al. (1997); (2) Vennes (1999); (3) Bergeron, Saffer, & Liebert (1992); (4) Liebert, Bergeron, & Holberg (2005); (5) Jordan et al. (1998); (6) Hillwig, Honeycutt, & Robertson (2000); (7) Dupuis et al. (1998); (8) Barstow et al. (1994); (9) Kawka et al. (2007); (10) Vennes, Korpela, & Bowyer (1997); (11) Schmidt et al. (1995).